THE MAPPING OF TECTONIC FEATURES IN THE OCEAN BASINS

FROM SATELLITE ALTIMETRY DATA

APPROVED:

_____

_____

_____

THE MAPPING OF TECTONIC FEATURES IN THE OCEAN BASINS FROM SATELLITE ALTIMETRY DATA

by

LISA MARIE GAHAGAN

THESIS

Presented to the Faculty of the Graduate School of

The University of Texas at Austin

in Partial Fulfillment

of the Requirements

for the Degree of

Master of Arts

THE UNIVERSITY OF TEXAS AT AUSTIN

May, 1988

Acknowledgements

I would like to thank all of the people who reviewed and commented on this thesis and the appendix. I would especially like to thank Chris Scotese, Larry Lawver, Jean-Yves Royer, and Dave Sandwell for all of their help. I would also like to thank Mark Cloos and John Sclater for their comments and suggestions. Many thanks to Dietmar Müller and Steve Cardimona for reading and proofing my thesis and for their encouragement when things looked down. It was great having these people as well as Cathy Mayes, Dirk Nürnberg, Lila Beckley, Debbie Lyle and Robynn Tomlins to lend their support. And, finally, a very big thank you to my husband, Alan, who endured the late nights and extra work (with only some complaining) and was a great support to me.

This work was supported by funding from Amoco International Oil Co., Chevron Overseas Petroleum Co., Conoco, Elf Aquitaine, Exxon Production Research, Mobil Oil Co., PetroCanada, Phillips Petroleum, Shell Development Co., and Standard Oil Co., as part of their sponsorship of the Paleoceanographic Mapping Project, University of Texas at Austin. This work was also partially supported by the NASA Geodynamics Program (NAG5-787).

THE MAPPING OF TECTONIC FEATURES IN THE OCEAN BASINS
FROM SATELLITE ALTIMETRY DATA

by

Lisa Marie Gahagan

Abstract

Satellite altimetry data provide information on the height variations of the sea surface. The angle between a line perpendicular to the sea surface and a vertical line between the satellite and the sea surface is referred to as the deflection of the vertical and is equal to the first derivative of the sea surface. This study examines two theoretical models describing the relationship between the deflection of the vertical data and the bathymetry 1) across a fracture zone in a large age-offset, fast-spreading regime and 2) across a fracture zone in a small age-offset, slow-spreading regime. The models are respectively compared to the observed relationship 1) across the Mendocino Fracture Zone which is in a large age-offset, fast-spreading regime and 2) across the DuToit Fracture Zone which is in a medium age-offset, slow-spreading regime. The strong agreement between the theoretical models and the observed relationships suggests that the models can be used with the deflection of the vertical data to locate fracture zones in known regimes.

The angle between the trend of a feature and the trend of the satellite track affects the deflection of the vertical signal. As the angle becomes smaller, the amplitude of the deflection of the vertical signal, which varies with the sine of this angle, decreases and the wavelength of the signal increases. Once the feature is parallel to the track, there is no deflection of the vertical signal.

The deflection of the vertical signal is also affected by the direction the satellite travels. If the feature trends between the ascending and descending tracks of the satellite, then the satellite will cross the feature from opposite directions and the ascending and descending signals will be opposite to each other. If the feature does not trend between the ascending and descending tracks, then the satellite will cross the feature from the same side and the deflection of the vertical signal will be similar for both the ascending and descending data sets.

A third factor affecting the deflection of the vertical signal is the latitude at which the feature is located. The trend of the satellite track varies as a function of latitude, ranging from 18° at 0° latitude to 64.6° at 70° latitude. Because the trend of the satellite track varies, not only does the angle between the trend of a feature and the trend of the satellite track vary with latitude, but the amplitude of the deflection of the vertical signal varies with latitude as well.

TABLE OF CONTENTS

I. Introduction

In 1978, NASA launched the Seasat satellite into a Earth orbit to collect various types of information about the Earth, such as wave height and winds at the sea surface (Lame and Born, 1982). As part of its operation, the satellite used a radar altimeter to measure the distance between itself and the sea surface. By subtracting this distance from the distance between the satellite and a calculated reference ellipsoid for the shape of the Earth, the height of the sea surface compared to the reference ellipsoid can be calculated (Tapley et al., 1982). To a first approximation, the sea surface can be compared to the equipotential gravitational surface known as the geoid (Sandwell, 1984a). Because the gravitational potential is the same at every point on this surface, the shape of the geoid, and hence the sea surface, changes to reflect gravity anomalies within the Earth. In areas of excess mass, the distance between the geoid and the mass increases so as to maintain the same gravitational potential. In areas where there is a deficit of mass, the distance between the surface of the geoid and the mass deficit decreases.

The geoid can be divided into long-wavelength and short-wavelength components which are interpreted, respectively, as deep-seated and shallow gravity anomalies. The short-wavelength component can be correlated with the bathymetry of the ocean floor (Haxby et al., 1983; Sandwell, 1984a). By using the satellite altimetry data to determine height variations in the sea surface, scientists have been able to detect bathymetric changes in the oceans basins and to obtain information on specific features in the oceans such as trenches (McAdoo, 1981), fracture zones (Sailor and Okal, 1983; Cande et al., in press), and seamounts (Craig and Sandwell, in press). Other researchers have used the data to examine the ocean basins from a more global perspective (Haxby, 1985; 1987; Gahagan et al., Appendix 1).

Changes in the average height of the sea surface across short-wavelength (<200 km) features, such as fracture zones, are on the order of one to two meters and extend over tens of kilometers. Because these subtle changes are often difficult to detect, the first derivative of the sea surface height has been used to enhance the short-wavelength component and hence reveal greater detail (Sandwell, 1984a). The first derivative is the slope between two points. From Figure 1a, the slope between points A and B is

Figure 1. a) The first derivative of the sea surface (geoid) between points A and B is equal to the slope between the points. The slope, y/x, is equal to the tangent of angle δ which approaches δ as δ becomes small. b) From geometry, the angle between a line perpendicular to the sea surface and the vertical line between the satellite and the sea surface is equal to δ. Thus the first derivative of the sea surface (geoid) is referred to as the deflection of the vertical.

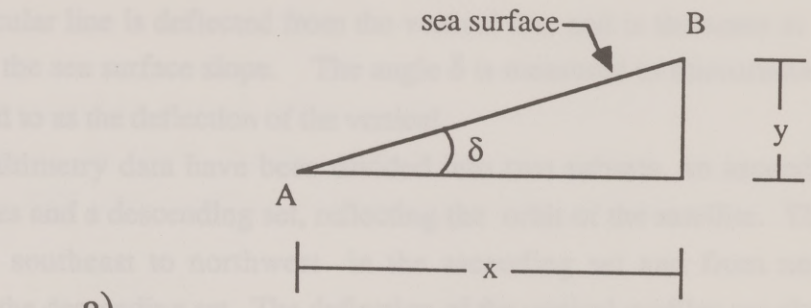
sea surface
B
δ
y
A
x

a)

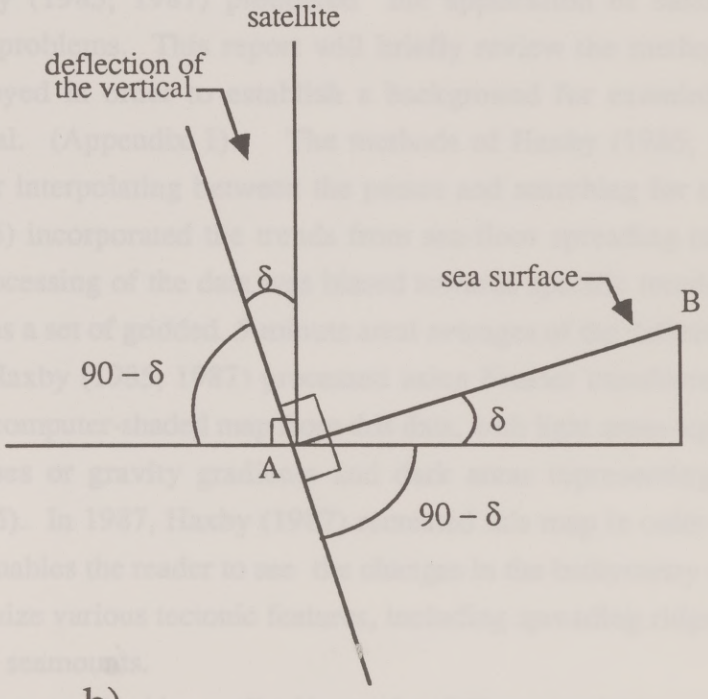
satellite
deflection of
the vertical
δ
sea surface
B
90 – δ
δ
A
90 – δ

b)

equal to y/x which is equal to tan δ. When δ is very small, tan $\delta \sim \delta$. The gravitational potential is directed perpendicular to the geoid and the sea surface. From the geometry in Figure 1b, the angle between the vertical line between the satellite and the sea surface and a line perpendicular to the sea surface is equal to δ. This angle is the distance that the perpendicular line is deflected from the vertical line and is the same as the first derivative of the sea surface slope. The angle δ is measured in microradians (μrads) and is referred to as the deflection of the vertical.

The altimetry data have been divided into two subsets, an ascending set of satellite passes and a descending set, reflecting the orbit of the satellite. The satellite travels from southeast to northwest in the ascending set and from northeast to southwest in the descending set. The deflection of the vertical profiles are plotted along the sub-tracks of the satellite (Figure 2). Lines connecting the peaks and troughs of the deflection of the vertical profiles would represent the maxima and minima, respectively, of the horizontal gravity associated with tectonic features on the ocean floor.

Haxby (1985; 1987) pioneered the application of satellite altimetry to geophysical problems. This report will briefly review the methods Haxby (1985; 1987) employed in order to establish a background for examining the work of Gahagan et al. (Appendix 1). The methods of Haxby (1985; 1987) included a technique for interpolating between the passes and searching for trends in the data. Haxby (1985) incorporated the trends from sea-floor spreading models so that the computer processing of the data was biased towards specific trends in certain areas. The result was a set of gridded, 5-minute areal averages of the deflection of the vertical data which Haxby (1985; 1987) processed using Fourier transforms. Haxby (1985) generated a computer-shaded map from this data, with light areas representing areas of positive slopes or gravity gradients and dark areas representing negative slopes (Haxby, 1985). In 1987, Haxby (1987) recreated this map in color. The shading on these maps enables the reader to see the changes in the bathymetry of the ocean floor and to recognize various tectonic features, including spreading ridges, fracture zones, trenches, and seamounts.

Gahagan et al. (Appendix 1) used a different technique of processing and interpreting the satellite altimetry data. First, they used Gaussian filters on the deflection of the vertical data to obtain a data set with wavelengths between 20 and 200

Figure 2. The ascending, filtered deflection of the vertical profiles are plotted along the satellite tracks in the North Pacific (after Sandwell, 1984b). MFZ = Mendocino Fracture Zone; PFZ = Pioneer Fracture Zone (from Gahagan et al., Appendix 1).

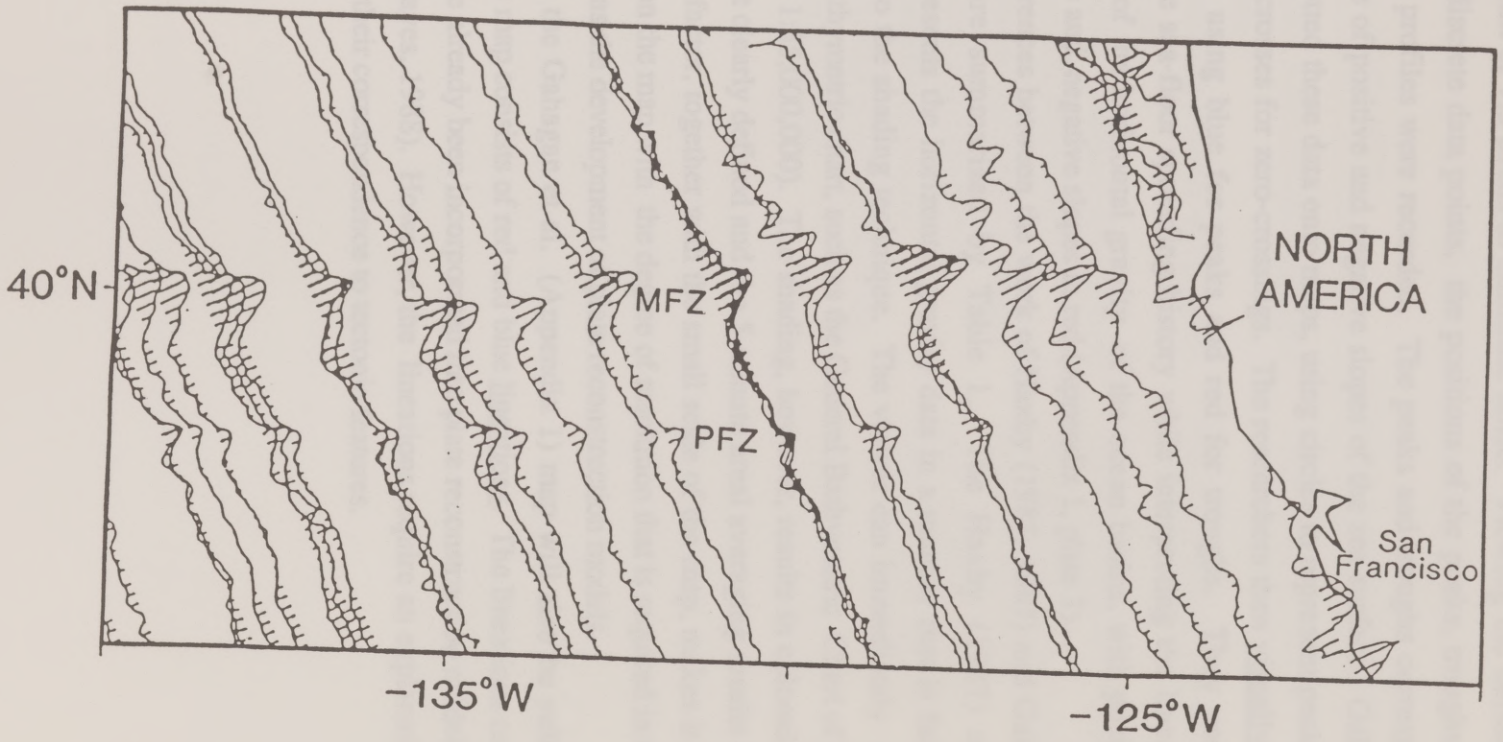
40°N
MFZ
PFZ
NORTH
AMERICA
San
Francisco
-135°W
-125°W

km (see Appendix 1 for more detail). In their processing, Gahagan et al. (Appendix 1) used a cut-off point of 7.5 μrads to eliminate noise. Viewing the deflection of the vertical data as discrete data points, the positions of the peaks, troughs, and zero-crossings on the profiles were recorded. The peaks and troughs correspond to the maximum degree of positive and negative slopes of the sea surface. Gahagan et al. (Appendix 1) plotted these data onto maps, using circles to represent peaks, triangles for troughs, and crosses for zero-crossings. The researchers then visually connected similar symbols using blue for peaks and red for troughs. They used a priori knowledge of the sea-floor spreading history while interpreting the lineations. The result is a map of the horizontal gravity of the ocean basins, with positive slopes delineated in blue and negative slopes in red (Appendix 1, plate 1).

The differences between the work of Haxby (1985; 1987) and Gahagan et al. (Appendix 1) are summarized by Table 1. The Haxby (1987) map (scale 1:40,000,000) presents the horizontal gravity data in a manner that is fairly easy to understand due to the shading technique. The viewer can immediately compare it visually with a bathymetric chart, such as the General Bathymetric Chart of the Oceans (GEBCO) (scale 1:35,000,000). The shading, however, results in colored areas with edges that are not clearly defined and the 5-minute areal averaging results in a loss in resolution. This factor, together with the small scale of the map, makes it difficult to digitize features on the map with the degree of resolution that is required in many types of research, such as the development of plate reconstruction models.

Although the Gahagan et al. (Appendix 1) map will also be published at a similar scale, this map consists of red and blue lineations. The lineations can be easily digitized and have already been incorporated into plate reconstruction models (Royer et al., submitted; Mayes, 1988). However, the lineations require an explanation of their derivation and of their correspondence to tectonic features.

Table 1

Differences between the work
of Haxby (1985; 1987) and Gahagan et al. (Appendix 1)

	Haxby (1985; 1987)	Gahagan et al. (Appendix 1)
1.	gridded, 5-minute areal averages of data	discrete data points
2.	Fourier-transformed the gridded data set	Gaussian-filtered the data points
3.	computer-generated shaded areas	visually interpreted lineations
4.	no tectonic interpretations	new tectonic interpretations
5.	resolution loss due to averaging	no resolution loss
6.	difficult to incorporate in reconstruction models due to lack of resolution of the tectonic features	easy to incorporate in reconstruction models

II. How to relate lineations in the deflection of the vertical charts and tectonic feature on the ocean floor

Upgrade the data and documentation

When Gahagan et al. (Appendix 1) began their research in mid-1986, the Seasat data were the best satellite altimeter data available. Unfortunately, the three-month long voyage of the Seasat satellite occurred during the Austral winter when the southern oceans are covered by ice. Consequently, the Seasat data south of 65°S are very noisy. In 1985, the U.S. Navy launched the Geosat satellite into an earth orbit. After completing its 18-month, classified primary mission, Geosat began collecting unclassified data. In January, 1987, the unclassified data from the first set of global repeat cycles of the Geosat mission were released. Gahagan et al. (Appendix 1) incorporated these data into their map in the southern oceans where the Seasat data were noisy. Interpretations south of 60°S were made using Geosat data. All other interpretations were made using Seasat data.

The work of Gahagan et al. (Appendix 1) can be use as the starting point for an improved horizontal gravity map based on Geosat data. Because of the better instrumentation on board the Geosat satellite, these data have better resolution and less noise than those of Seasat (MacArthur et al., 1987; Sailor and LeSchack, 1987; Sandwell and McAdoo, in press). Seasat had a short wavelength resolution of 50 km and a total root mean square noise (RMS) level of 10.6 μrads which is equivalent to 8.4 cm (Marks and Sailor, 1986). Geosat has a short wavelength resolution of 25 to 45 km and a total RMS of 2 to 3 μrads or about 3 cm (Sandwell and McAdoo, in press). The Geosat satellite was placed in a 17-day orbit similar to the Seasat orbit for the unclassified part of its mission (Jensen and Wooldridge, 1987; McConathy and Kilgus, 1987). From this part of the mission which is known as the Exact Repeat Mission, the ground tracks from Geosat's repeat orbits are within ± 1 km of each other (Born et al., 1987). Seasat collected one global data set with an equatorial track-spacing of 165 km and 8 repeat orbit sets with an equatorial track-spacing of 900 km (Tapley et al., 1982). During its operation, Geosat has made over 20 sets of repeat orbits with an equatorial spacing of 165 km (Sandwell, pers. comm). The Geosat

repeat orbits can be stacked and averaged together to produce a data set with a much higher resolution than available with Seasat.

The first step in producing the new map is to filter the Geosat deflection of the vertical data and plot it at the scale of the GEBCO charts so that the two data bases can be overlain and directly compared (Figure 3a and b). The lineations through the peaks and troughs could be digitized with control points directly on the satellite sub-track (Figure 3c). The lineations can be plotted out at GEBCO scale. Having both the deflection of the vertical data and the interpretations at GEBCO scale will allow researchers to go back to the three databases, compare them and see exactly how an interpretation was made, and to change that interpretation if necessary.

Establish the observational relationship between bathymetry and the deflection of the vertical signal

Researchers have shown that a correlation exists between the short wavelength component of the geoid and the bathymetry of the ocean floor (Haxby et al., 1983; Sandwell, 1984a; Gahagan et al., Appendix 1). Sandwell (1984a) processed the Geos-3 and Seasat deflection of the vertical data and used a hill shading technique to produce a map of the South Pacific similar to Haxby's (1985). By comparing the major features on his map to those features on the Mammerickx et al. (1974) bathymetric chart of the South Pacific, Sandwell (1984a) showed that a correlation existed between his processed data and the bathymetry. Sandwell (1984a) presented both his map and the Mammerickx et al. (1974) chart in his paper which also enabled the reader to compare them.

One of the questions that arises upon examining the Gahagan et al. (Appendix 1) map is "How do these red and blue lineations correspond to tectonic features and ocean floor bathymetry?". Once a correlation has been shown to exist between the horizontal gravity map and GEBCO bathymetry, the lineations can be used to identify previously unknown features or to extend the length of features into areas where bathymetric data is lacking, such as in the southern oceans. These lineations can then be used in conjunction with the known bathymetry, earthquake data and marine magnetic anomaly data to map the tectonic features of the ocean basins. To do this effectively, models must be developed describing the relationship between

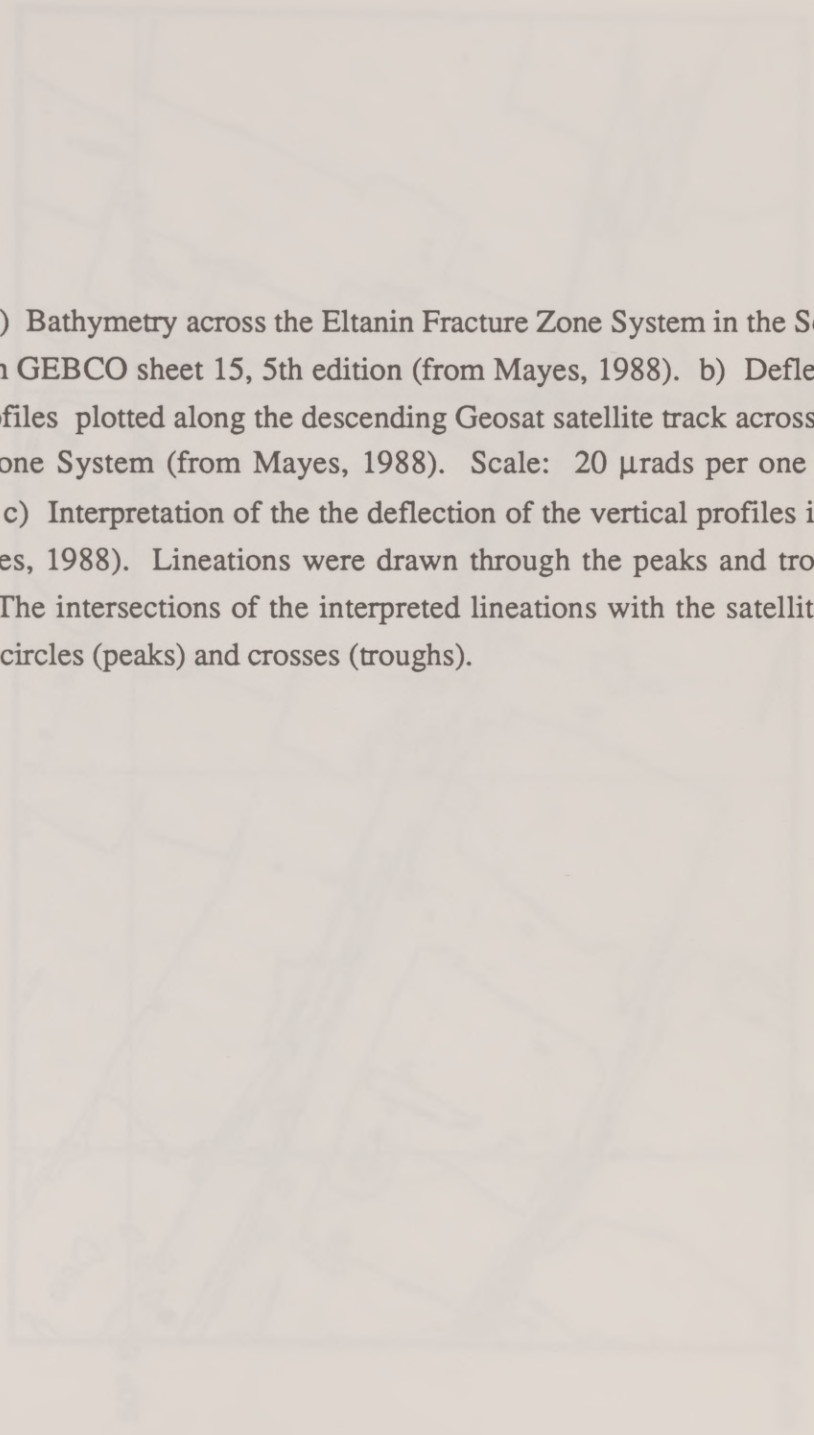

Figure 3. a) Bathymetry across the Eltanin Fracture Zone System in the South Pacific Ocean from GEBCO sheet 15, 5th edition (from Mayes, 1988). b) Deflection of the vertical profiles plotted along the descending Geosat satellite track across the Eltanin Fracture Zone System (from Mayes, 1988). Scale: 20 μrads per one degree of longitude. c) Interpretation of the the deflection of the vertical profiles in Figure 3b (after Mayes, 1988). Lineations were drawn through the peaks and troughs of the profiles. The intersections of the interpreted lineations with the satellite tracks are marked by circles (peaks) and crosses (troughs).

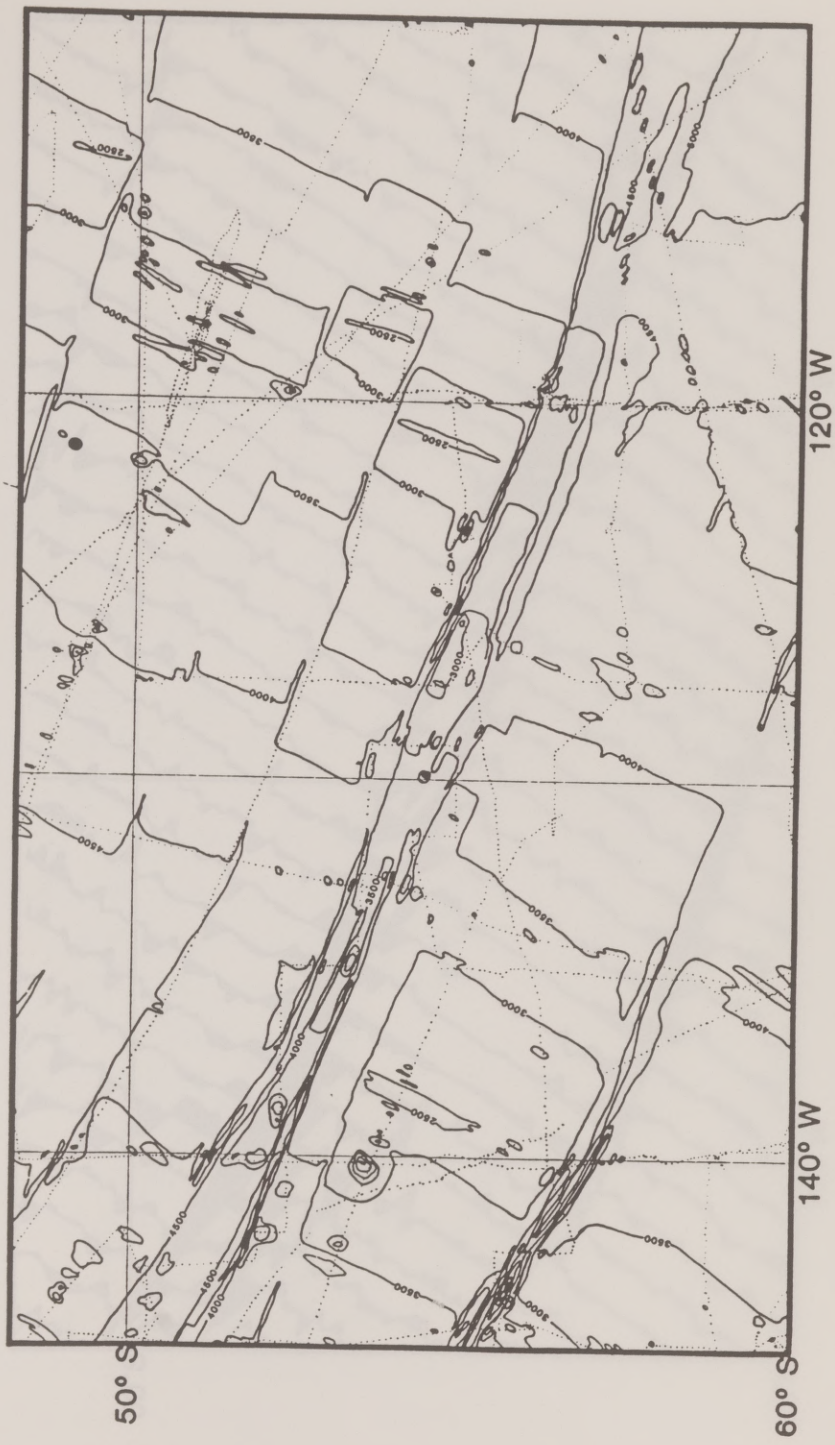

a)

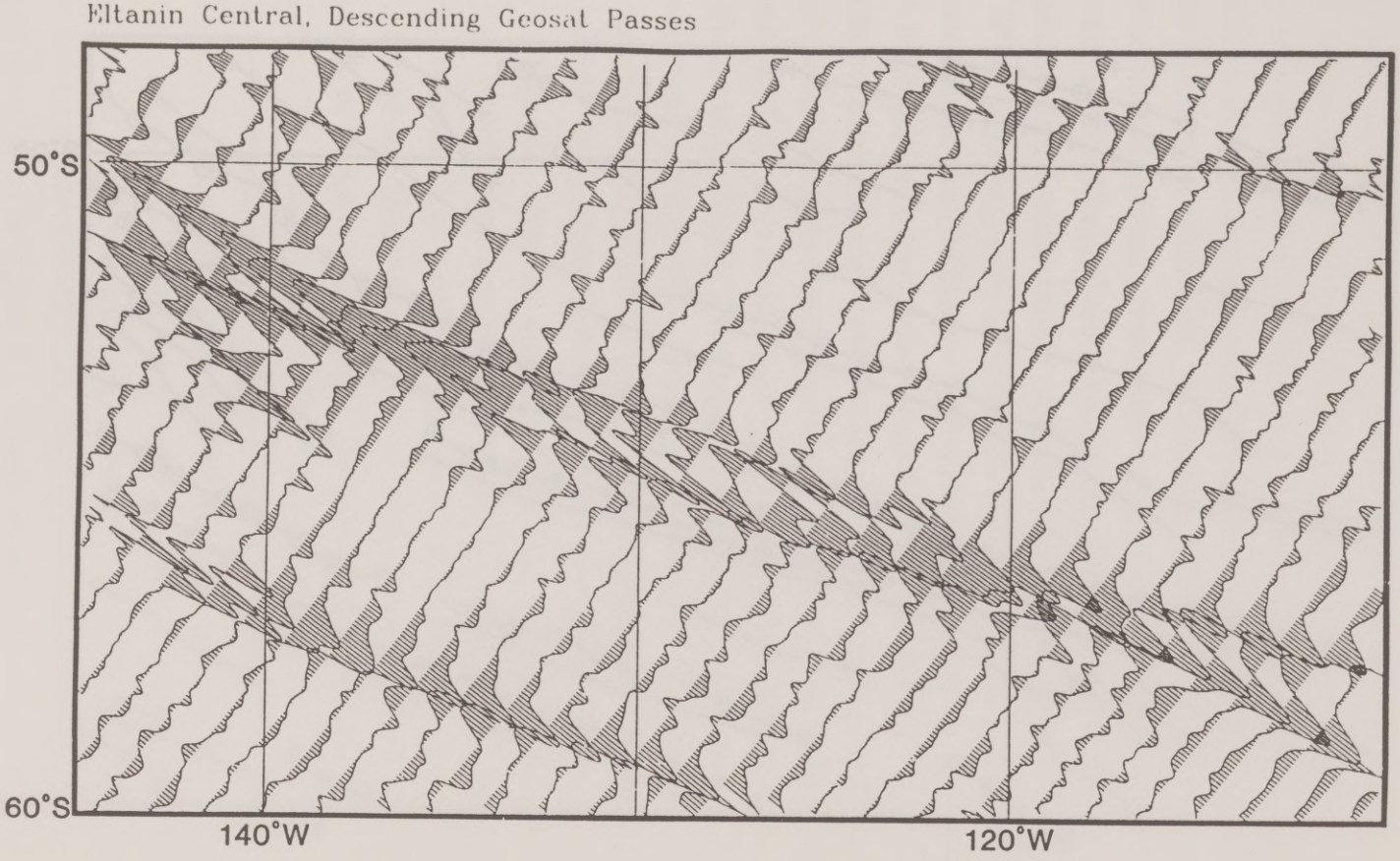
Eltanin Central, Descending Geosat Passes
50°S
60°S
140°W
120°W

b)

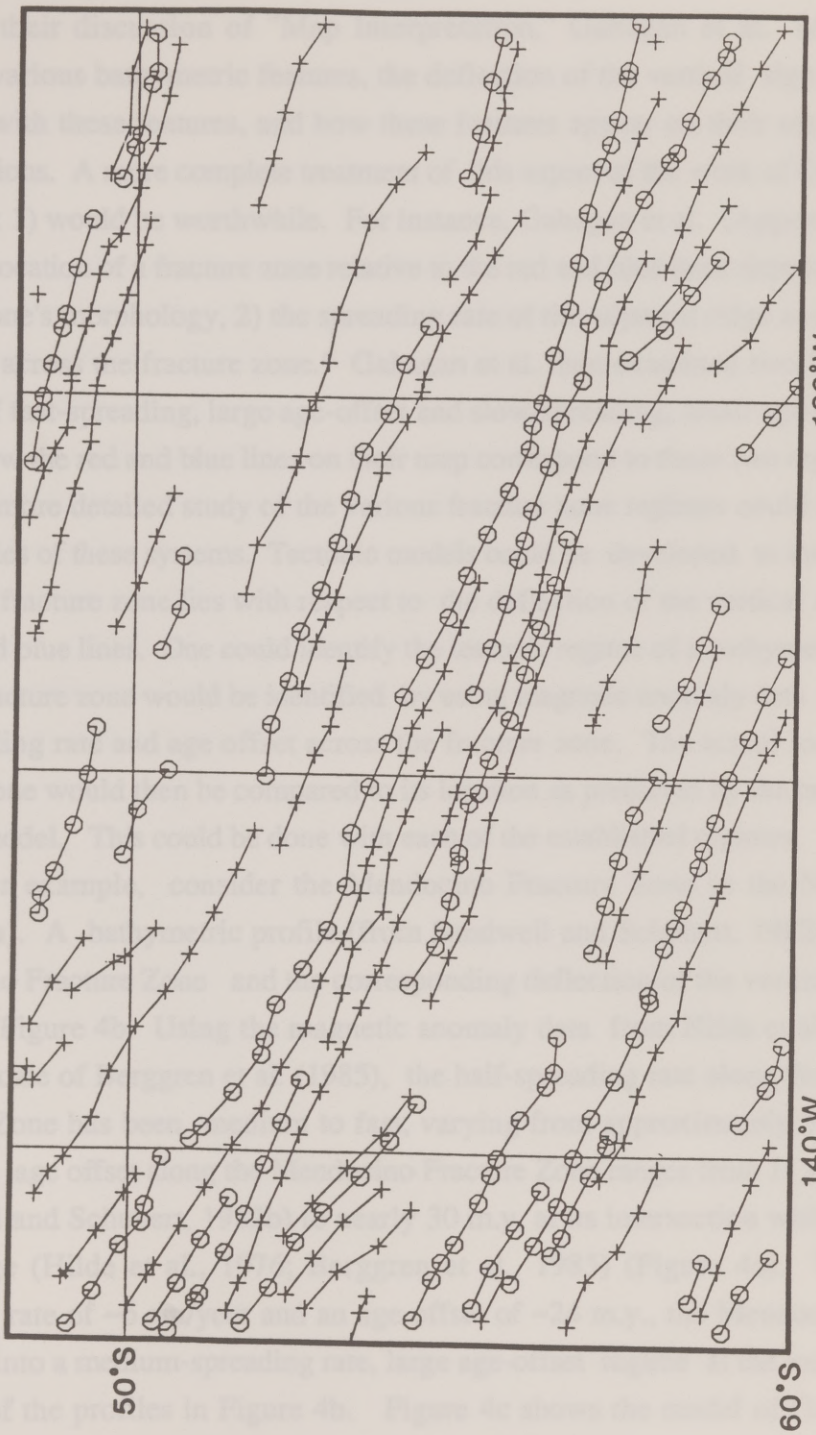

c)

the bathymetry and the red and blue lineations.

In their discussion of "Map Interpretation," Gahagan et al. (Appendix 1) reviewed various bathymetric features, the deflection of the vertical signal one might associate with these features, and how these features appear on their map as red and blue lineations. A more complete treatment of this aspect of the work of Gahagan et al. (Appendix 1) would be worthwhile. For instance, Gahagan et al. (Appendix 1) stated that "The location of a fracture zone relative to the red and blue lines depends on: 1) the fracture zone's morphology, 2) the spreading rate of the adjacent ridge axis, and 3) the age offset across the fracture zone." Gahagan et al. then examined two fracture zone regimes of fast-spreading, large age-offset and slow-spreading, small age-offset. They explain how the red and blue lines on their map correspond to these two regimes.

A more detailed study of the various fracture zone regimes could illustrate the complexities of these systems. Tectonic models could be developed to interpret where the actual fracture zone lies with respect to the deflection of the vertical signal and to the red and blue lines. One could identify the tectonic regime of a bathymetrically well-defined fracture zone would be identified by using magnetic anomaly data to determine the spreading rate and age offset across the fracture zone. The actual location of the fracture zone would then be compared to its location as predicted by the corresponding tectonic model. This could be done with each of the established regimes.

For example, consider the Mendocino Fracture Zone in the North Pacific (Figure 4a). A bathymetric profile (from Sandwell and Schubert, 1982a) across the Mendocino Fracture Zone and the corresponding deflection of the vertical profile are shown in Figure 4b. Using the magnetic anomaly data from Hilde et al. (1976) and the time scale of Berggren et al. (1985), the half-spreading rate along the Mendocino Fracture Zone has been medium to fast, varying from approximately 3 to 7 cm per year. The age offset along the Mendocino Fracture Zone ranges from 11 m.y. at 180°E (Sandwell and Schubert, 1982b) to nearly 30 m.y. at its intersection with the Juan de Fuca ridge (Hilde et al., 1976; Berggren et al., 1985) (Figure 4a). With a half-spreading rate of ~6 cm/year and an age offset of ~24 m.y., the Mendocino Fracture Zone fits into a medium-spreading rate, large age-offset regime at the location (40°N, 133°W) of the profiles in Figure 4b. Figure 4c shows the model of Gahagan et al. (Appendix 1) for a fracture zone in a fast-spreading, large age-offset regime.

Figure 4. a) Map of the Northeast Pacific Ocean showing the location of five bathymetric profiles across the Mendocino and Pioneer fracture zones (after Sandwell and Schubert, 1982a). JF = Juan de Fuca Ridge. b) Bathymetric profile B from Figure 4a (Sandwell and Schubert, 1982a) and deflection of the vertical profile across the Mendocino (MFZ) and Pioneer (PFZ) fracture zones in the North Pacific Ocean. The bathymetric profile is a north-south profile located at ~133°W. The spreading rate along the Mendocino Fracture Zone was a medium- to fast-spreading rate, and the age offset at the point crossed by the bathymetric profile is ~24 m.y. (Hilde et al., 1976; Berggren et al., 1985). c) Theoretical model describing the deflection of the vertical profile expected across a fracture zone in a fast-spreading, large age-offset regime (after Gahagan et al., Appendix 1).

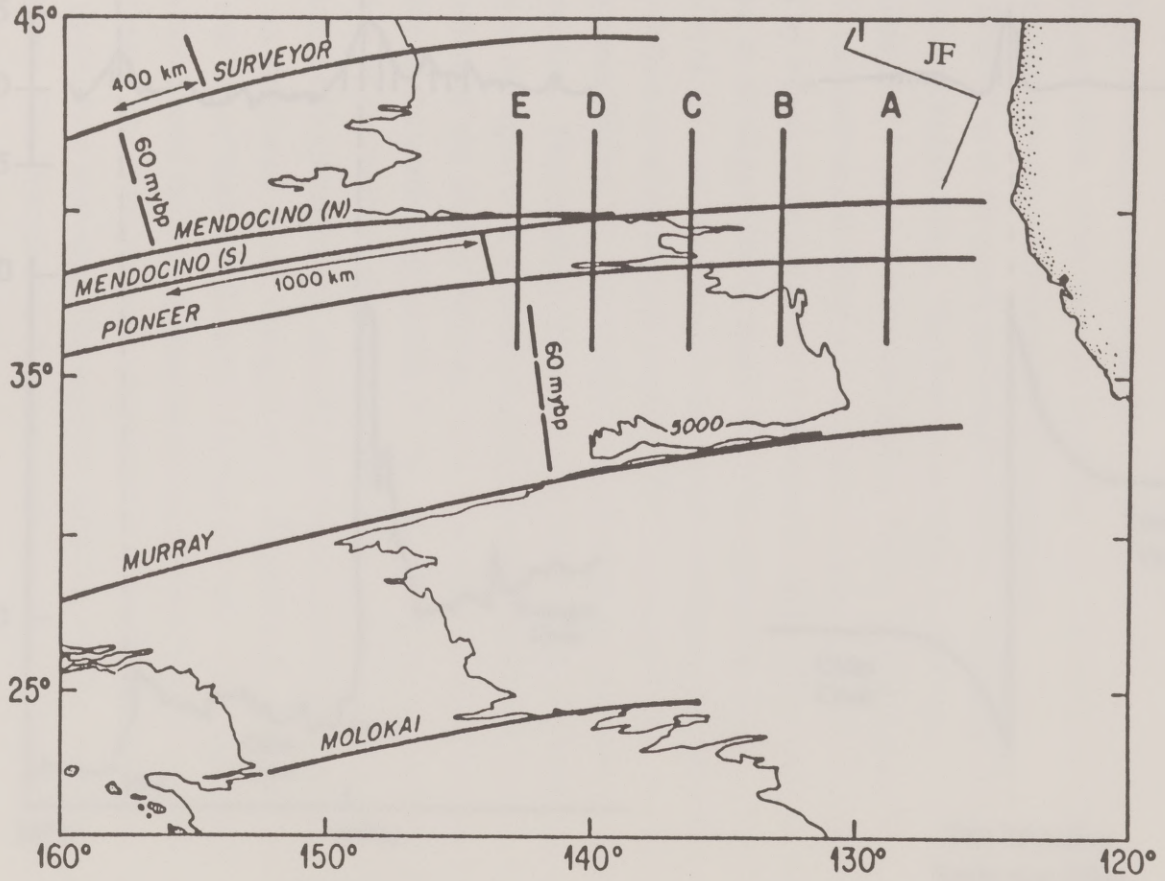
45°
35°
25°
160°
150°
140°
130°
120°
400 km
SURVEYOR
60 mybp
MENDOCINO (N)
MENDOCINO (S)
1000 km
PIONEER
JF
E
D
C
B
A
60 mybp
3000
MURRAY
MOLOKAI

a)

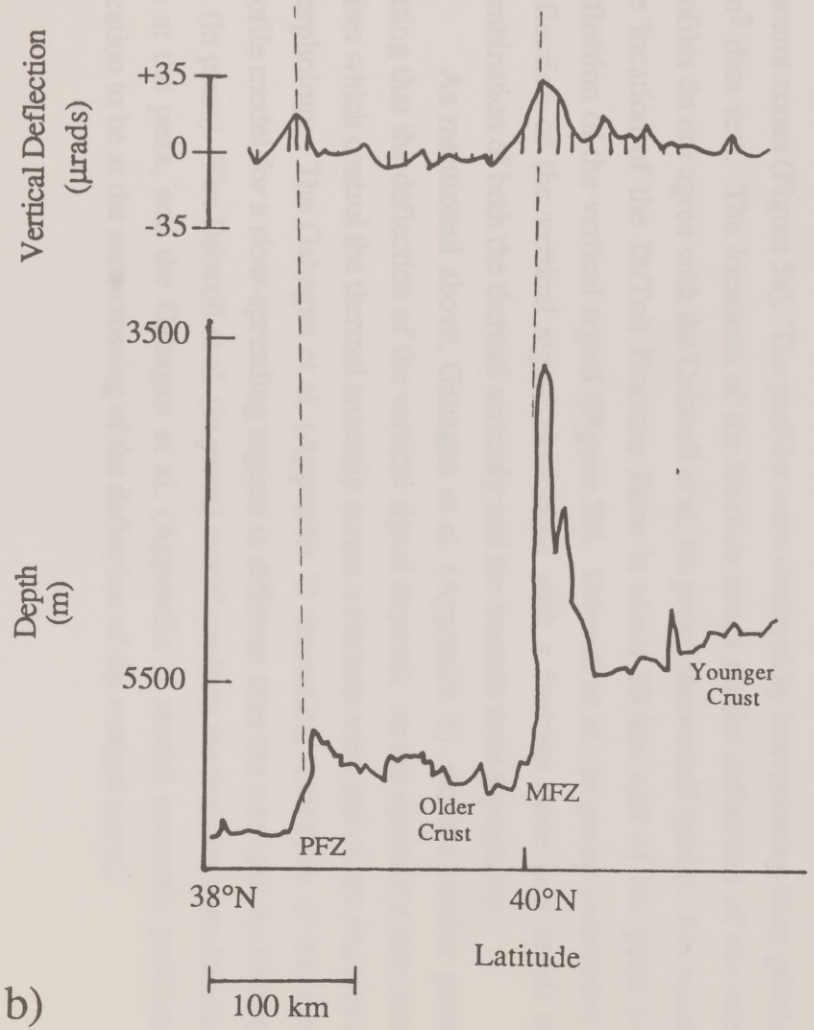
Vertical Deflection
(μrads)
+35
0
-35
3500
Depth
(m)
5500
Younger
Crust
Older
Crust
MFZ
PFZ
38°N
40°N
Latitude
100 km

b)

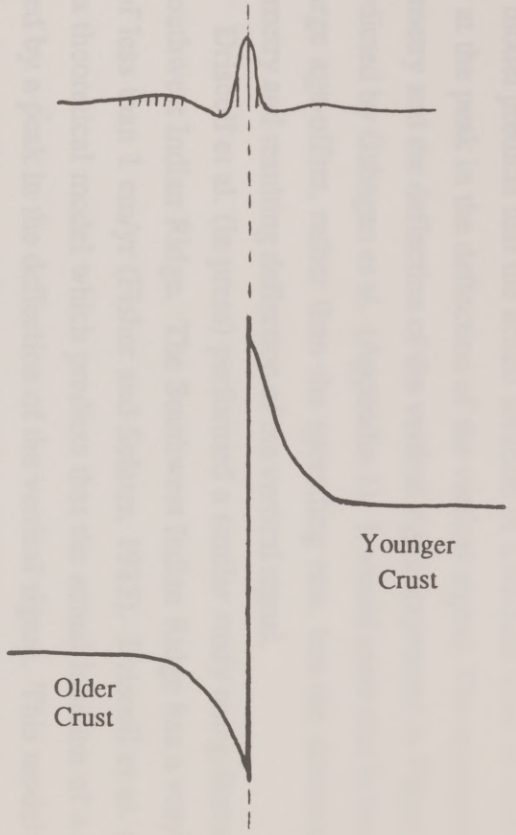
Younger
Crust
Older
Crust
Fast Spreading
Large Age Offset
Fracture Zone

c)

Their model predicts that the actual location of a fracture zone in such a regime would occur at the peak in the deflection of the vertical signal. The relationship between the bathymetry and the deflection of the vertical signal expressed in Figure 4b is as exactly as predicted by Gahagan et al. (Appendix 1). It would seem that in this particular case, the large age-offset, rather than the spreading rate, has the dominant effect on the bathymetry and resulting deflection of the vertical signal.

Driscoll et al. (in press) performed a similar study using fracture zones across the Southwest Indian Ridge. The Southwest Indian Ridge has a very slow spreading rate of less than 1 cm/yr (Fisher and Sclater, 1983). Driscoll et al. (in press) began with a theoretical model which predicts that the actual location of a fracture zone is marked by a peak in the deflection of the vertical signal. This model is similar to the Gahagan et al. (Appendix 1) model for a fast-spreading, large age-offset regime. Driscoll et al. (in press) compared twelve profiles displaying the bathymetry, the geoid, and the deflection of the vertical across the DuToit, Andrew Bain, and Prince Edward fracture zones (Figure 5a). The profiles were obtained by interpolating from gridded, 8 km^2 data sets. The locations of the fracture zones on the deflection of the vertical profiles do not agree with the Driscoll et al. (in press) theoretical model. For example, the location of the DuToit Fracture Zone is about 10 km east of the peak in the deflection of the vertical signal (Figure 5b). Driscoll et al. (in press) concluded that deflection of the vertical signal associated with a fracture zone is a result of "a combination of both the thermal anomaly and the fracture zone topography."

As mentioned above, Gahagan et al. (Appendix 1) made a similar point by stating that the deflection of the vertical signal depends on the spreading rate and age offset which control the thermal anomaly across a fracture zone and on the fracture zone morphology. The Gahagan et al. (Appendix 1) theoretical deflection of the vertical profile model for a slow-spreading regime is different than the one used by Driscoll et al. (in press). The Driscoll et al. (in press) model predicts the fracture zone location to be at the peak, and the Gahagan et al. (Appendix 1) model correctly predicts the location to be at the zero-crossing of the deflection of the vertical signal.

Figure 5. a) Map locating twelve profiles across the DuToit, Andrew Bain, and Prince Edward fracture zones in the Southwest Indian Ocean. Solid circles indicate earthquake epicenters along the Southwest Indian Ridge (from Figure 8, Driscoll et al., in press). b) Profiles (AA' on Figure 5a) of the bathymetry, geoid, and deflection of the vertical across the DuToit (DT) and Andrew Bain (AB) (from Figure 9, Driscoll et al., in press). The southeast-northwest trending profiles cross the DuToit Fracture Zone at approximately 53°S, 24°E. The profiles parallel a segment of the Southwest Indian Ridge which is located to the left of the DuToit Fracture Zone on the profiles and accounts for the "high" seen on the bathymetric and geoid profiles. The spreading rate along the DuToit Fracture Zone has been less than 1 cm/yr (Fisher and Sclater, 1983). c) Theoretical model describing the deflection of the vertical profile expected across a fracture zone in a slow-spreading, small age-offset regime (from Gahagan et al., Appendix 1).

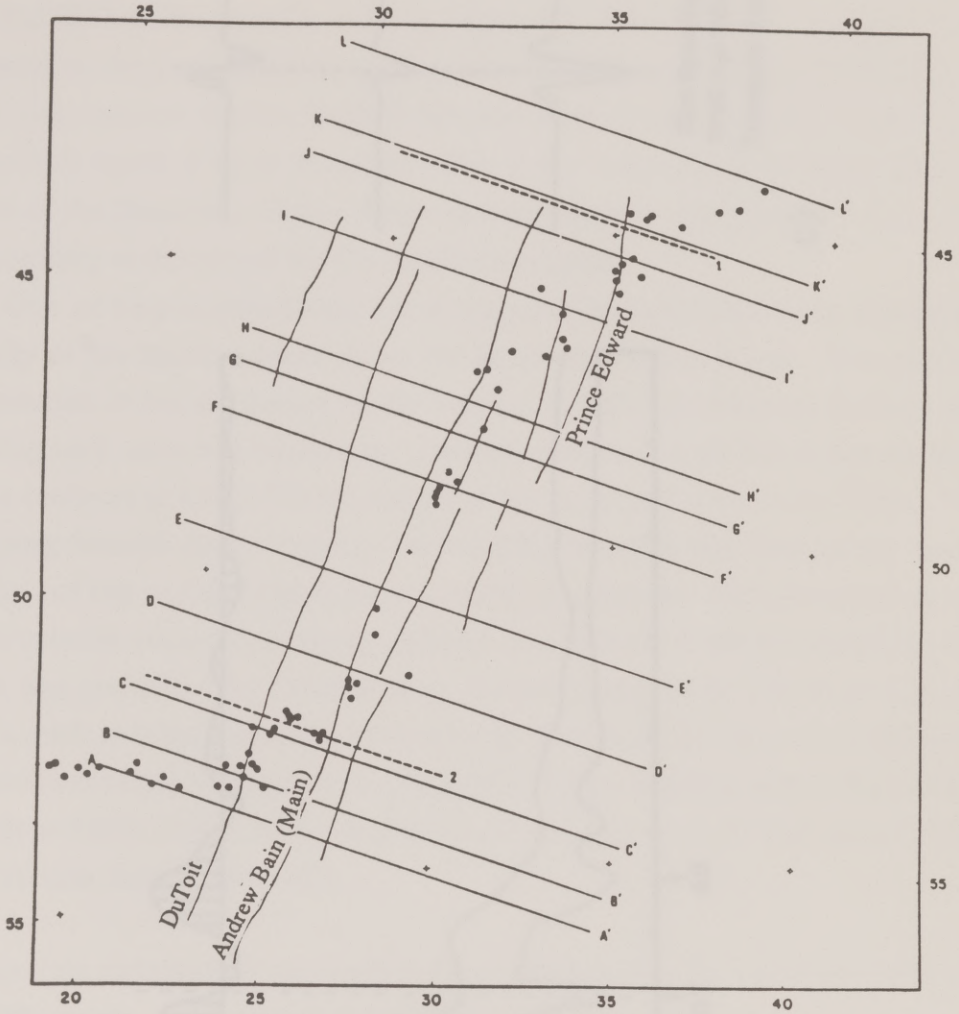
25
30
35
40
45
50
55
20
L
K
J
I
H
G
F
E
D
C
B
A
L'
K'
J'
I'
H'
G'
F'
E'
D'
C'
B'
A'
1
2
Prince Edward
DuToit
Andrew Bain (Main)

a)

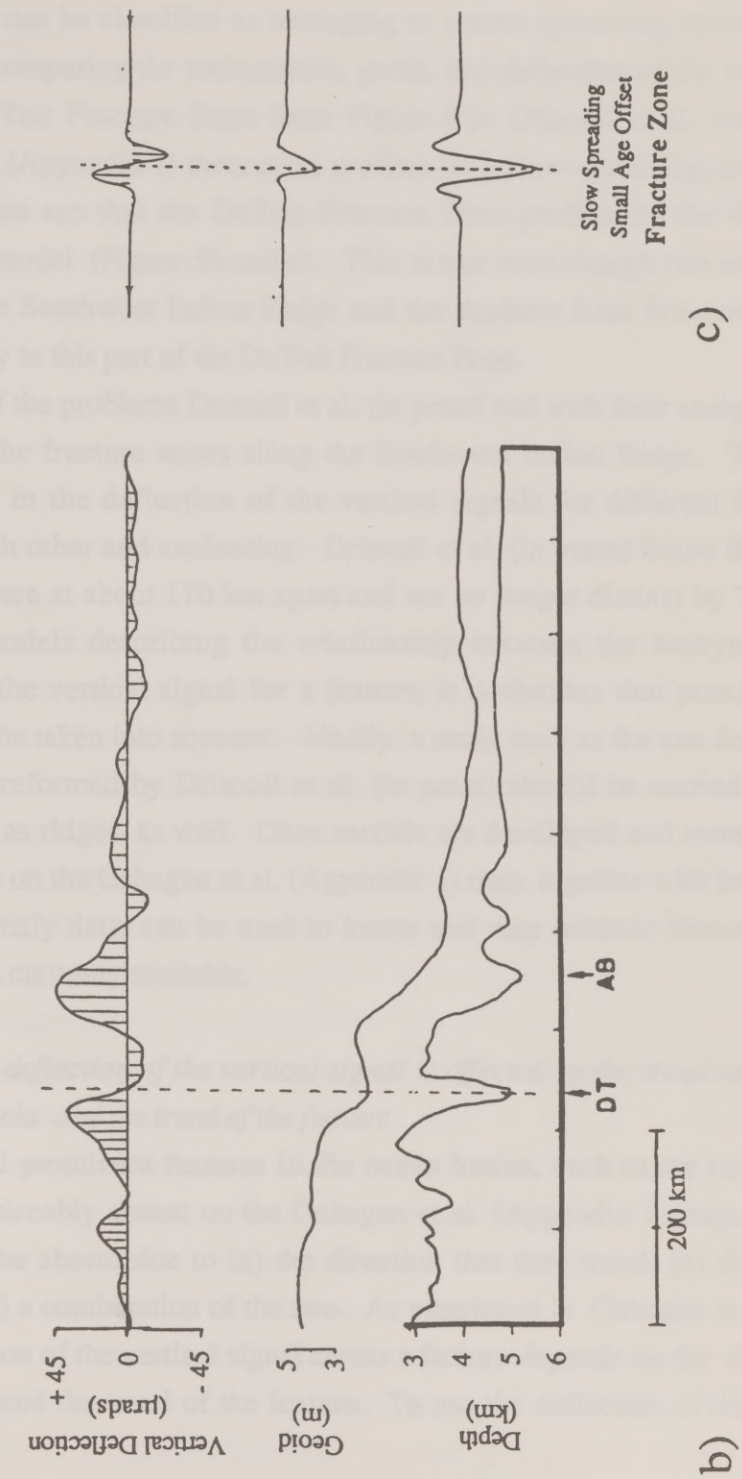
Slow Spreading
Small Age Offset
Fracture Zone
c)
Vertical Deflection
(μrads)
+45
0
-45
Geoid
(m)
5
3
Depth
(km)
3
4
5
6
DT
AB
200 km
b)

With an age offset of about 12 m.y. (Driscoll et al., in press), the DuToit Fracture Zone can be classified as belonging to a slow-spreading, medium age-offset regime. By comparing the bathymetric, geoid, and deflection of the vertical profiles across the DuToit Fracture Zone from Figure 9 in Driscoll et al. (in press) to the Gahagan et al. (Appendix 1) theoretical profiles for a slow-spreading, small age-offset regime, one can see that the DuToit Fracture Zone profiles fit the Gahagan et al. (Appendix 1) model (Figure 5b and c). This is true even though two other features, a segment of the Southwest Indian Ridge and the Andrew Bain Fracture Zone, are in close proximity to this part of the DuToit Fracture Zone.

One of the problems Driscoll et al. (in press) had with their study was the close proximity of the fracture zones along the Southwest Indian Ridge. This proximity often resulted in the deflection of the vertical signals for different fracture zones overriding each other and coalescing. Driscoll et al. (in press) found that the signals begin to coalesce at about 170 km apart and are no longer distinct by 70 km. When developing models describing the relationship between the bathymetry and the deflection of the vertical signal for a feature, it is obvious that proximity to other features must be taken into account. Ideally, a study such as the one described above and the one preformed by Driscoll et al. (in press) should be carried out for other features, such as ridges, as well. Once models are developed and tested, the red and blue lineations on the Gahagan et al. (Appendix 1) map, together with bathymetric and magnetic anomaly data, can be used to locate and map tectonic features at a higher resolution than currently available.

Study how the deflection of the vertical signal is affected by the trend and direction of the satellite tracks and the trend of the feature

Several prominent features in the ocean basins, such as the ocean spreading ridges, are noticeably absent on the Gahagan et al. (Appendix 1) map. Some of the features may be absent due to (a) the direction that they trend, (b) data processing methods, or (c) a combination of the two. As mentioned in Gahagan et al. (Appendix 1), the deflection of the vertical signal across a feature depends on the direction of the satellite track and the trend of the feature. To use the deflection of the vertical data

effectively, one must understand how changes in these trends can affect the deflection of the vertical signal.

Consider the angle α between the trend of a feature and the trend of the satellite track (Figure 6). The amplitude of the deflection of the vertical signal reaches a maximum value when a feature is perpendicular to the track (Figure 6a). As the angle α becomes smaller, the width of the signal broadens and the amplitude of the deflection of the vertical signal becomes smaller (Figure 6b). The relationship between the angle α and the amplitude of the deflection of the vertical signal can be expressed by:

$$a_\alpha = (A_{max})\sin \alpha \qquad (1)$$

where a_α = amplitude of the deflection of the vertical at angle α

α = angle between the feature and the satellite track

A_{max} = maximum amplitude at $\alpha = 90°$

The amplitude reaches a maximum at $\alpha = 90°$. When $\alpha = 0°$, the feature and the track are parallel and the amplitude is equal to zero (Figure 6c).

The above relationship explains why some features which were parallel the trend of the satellite track were not recognized on the Gahagan et al. (Appendix 1) map. For instance, the amplitude of the deflection of the vertical signal across the Mendocino Fracture Zone is approximately 35 µrads (Figure 4a). The angle between the Mendocino Fracture Zone and the ascending satellite track is ~64° (see equation 2). From equation (1), if this angle were 90°, the maximum amplitude would be ~39 µrads. If the angle were 11°, the amplitude would only be 7.44 µrads which is less than the 7.5 µrads noise cut-off point used by Gahagan et al. (Appendix 1). Therefore, such a feature, even if it had as large an amplitude as the Mendocino Fracture Zone, would not appear in the Gahagan et al. (Appendix 1) ascending data set if the angle between the feature and the ascending track were 11° or less. Although the feature might appear on the descending tracks, it may not be a traceable, coherent feature without the data on the ascending tracks.

As mentioned above, the direction (ascending or descending) of the satellite also affects the deflection of the vertical signal across a feature. The polar orbit of the satellite results in northwest-trending, ascending tracks or southwest-trending,

Figure 6. a) The amplitude of the deflection of the vertical signal across a feature, such as a fracture zone (FZ), reaches a maximum point when the feature is perpendicular to the satellite track. b) As the angle between the track and the feature becomes smaller, the deflection of the vertical signal broadens and the amplitude of the signal decreases. c) The amplitude of the deflection of the vertical signal is a function of the sine of the angle (α) between the feature and the satellite track.

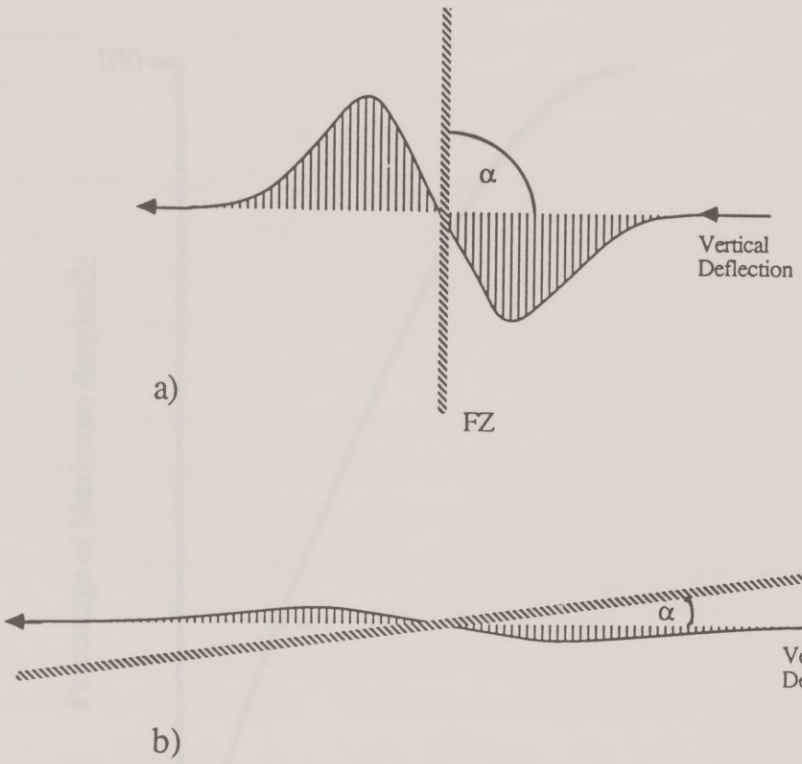
α
Vertical
Deflection
a)
FZ
FZ
α
Vertical
Deflection
b)

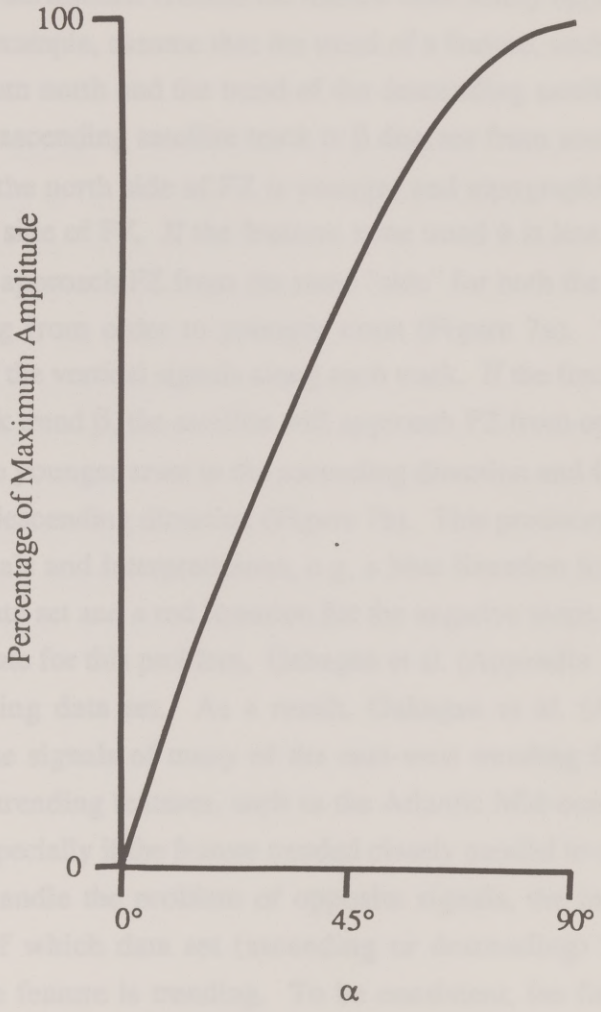

c)

descending tracks. These track trends enhance the signals over east-west trending features which intersect the tracks at large angles. However, when the ascending and descending tracks are used together, the tracks may present a disadvantage when interpreting east-west trending signals. The ascending profile across an east-west trending feature will have the opposite signal of the descending profile across that feature since the satellite crossed the feature from nearly opposite directions.

For example, assume that the trend of a feature, such as a fracture zone (FZ), is ϕ degrees from north and the trend of the descending satellite track is β degrees from north. (The ascending satellite track is β degrees from south, Figure 7) Assume that the crust on the north side of FZ is younger and topographically higher than the crust on the south side of FZ. If the fracture zone trend ϕ is less than the track trend β, the satellite will approach FZ from the same "side" for both the ascending and descending paths, going from older to younger crust (Figure 7a). This will produce similar deflection of the vertical signals along each track. If the fracture zone trend ϕ is greater than the track trend β, the satellite will approach FZ from opposite "sides," going from older crust to younger crust in the ascending direction and from younger crust to older crust in the descending direction (Figure 7b). This produces opposite deflection of the vertical signals and interpretations, e.g. a blue lineation for the positive slope on the ascending data set and a red lineation for the negative slope on the descending data set. To compensate for this problem, Gahagan et al. (Appendix 1) switched the symbols on the descending data set. As a result, Gahagan et al. (Appendix 1) were able to recognize the signals of many of the east-west trending fracture zones. This made north-south trending features, such as the Atlantic Mid-ocean Ridge, more difficult to recognize especially if the feature trended closely parallel to one of the satellite tracks.

To handle the problem of opposite signals, the interpreter must always be conscious of which data set (ascending or descending) he is using and of which direction the feature is trending. To be consistent, the final output map should be produced as if all the features were being viewed from one direction, ascending or descending. A safe "rule" to follow is that if the signal on a deflection of the vertical profile is pointing westward, the signal is indicating a negative slope from the ascending point of view. If the signal points eastward, it is indicating a positive slope from the ascending point of view.

Figure 7. A feature, such as a fracture zone (FZ), is crossed by both the ascending (A) and descending (D) satellite tracks. FZ trends ϕ degrees from north. The crust north of FZ is younger than the crust to the south. The descending track trends β degrees from north and the ascending track trends 360-β degrees from north, or Sβ°E. The angle between FZ and the descending track is α. a) If $\phi < \beta$, the satellite will approach FZ from the same side, crossing from older crust to younger crust. The ascending and descending deflection of the vertical profiles across FZ will be similar. b) If $\phi > \beta$, the satellite will approach FZ from "opposite" sides, crossing from older crust to younger crust in the ascending direction and from younger crust to older crust in the descending direction. The deflection of the vertical profiles will be different since the ascending profile will show a positive slope and the descending profile will show a negative slope.

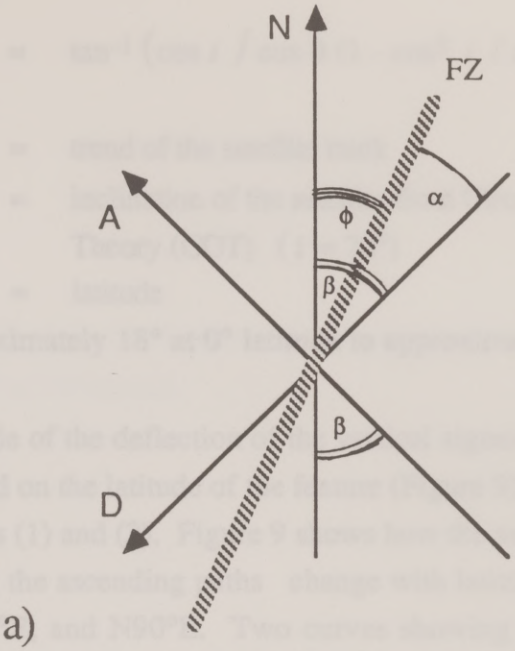

a)

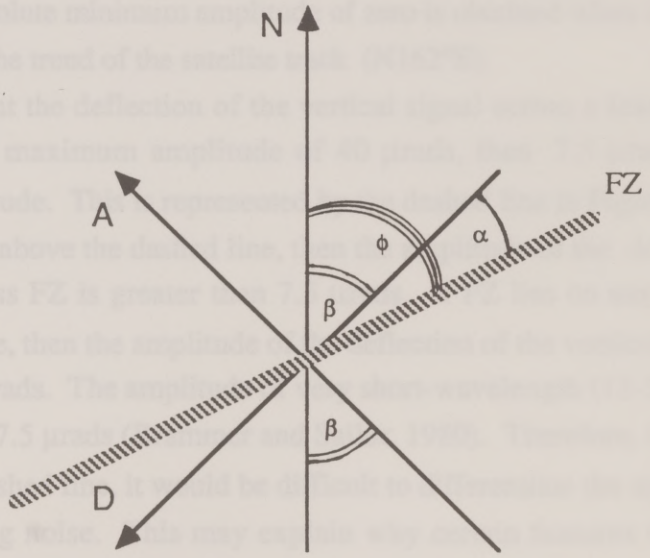

b)

$$\beta = \tan^{-1}\left(\cos i \,/\, \cos\theta\,(1 - \cos^2 i \,/\, \cos^2\theta)^{.5}\right) \qquad (2)$$

where β = trend of the satellite track

i = inclination of the satellite from Circular Orbit Theory (COT) ($i = 72°$)

θ = latitude

β varies from approximately 18° at 0° latitude to approximately 64.6° at 70° latitude (Figure 8.)

The amplitude of the deflection of the vertical signal across a feature depends both on the trend and on the latitude of the feature (Figure 9) and can be calculated by combining equations (1) and (2). Figure 9 shows how the amplitude of the deflection of the vertical along the ascending paths change with latitude for features that trend N0°E, N30°E, N60°E, and N90°E. Two curves showing when the minimum and maximum amplitudes are obtained for a feature located at the equator are also plotted on the diagrams. As expected, the absolute maximum amplitude on an ascending profile is obtained when the trend of the feature is perpendicular to the trend of the satellite track (N72°E), and the absolute minimum amplitude of zero is obtained when the trend of the feature is parallel to the trend of the satellite track (N162°E).

Assuming that the deflection of the vertical signal across a feature, FZ, has a very large absolute maximum amplitude of 40 μrads, then 7.5 μrads is equal to 18.75% of the amplitude. This is represented by the dashed line in Figure 9. If FZ lies on any of the curves above the dashed line, then the amplitude of the deflection of the vertical profile across FZ is greater than 7.5 μrads. If FZ lies on any of the curves below the dashed line, then the amplitude of the deflection of the vertical profile across FZ is less than 7.5 μrads. The amplitude of very short-wavelength (13-33 km) noise is slightly greater than 7.5 μrads (Brammer and Sailor, 1980). Therefore, if FZ did lie on a curve below the dashed line, it would be difficult to differentiate the signal across FZ from the surrounding noise. This may explain why certain features that one might expect to recognize using the deflection of the vertical data are not seen.

Figure 8. The trend β of the satellite track is a function of latitude. β ranges from 18° at 0° latitude to 64.6° at 70° latitude.

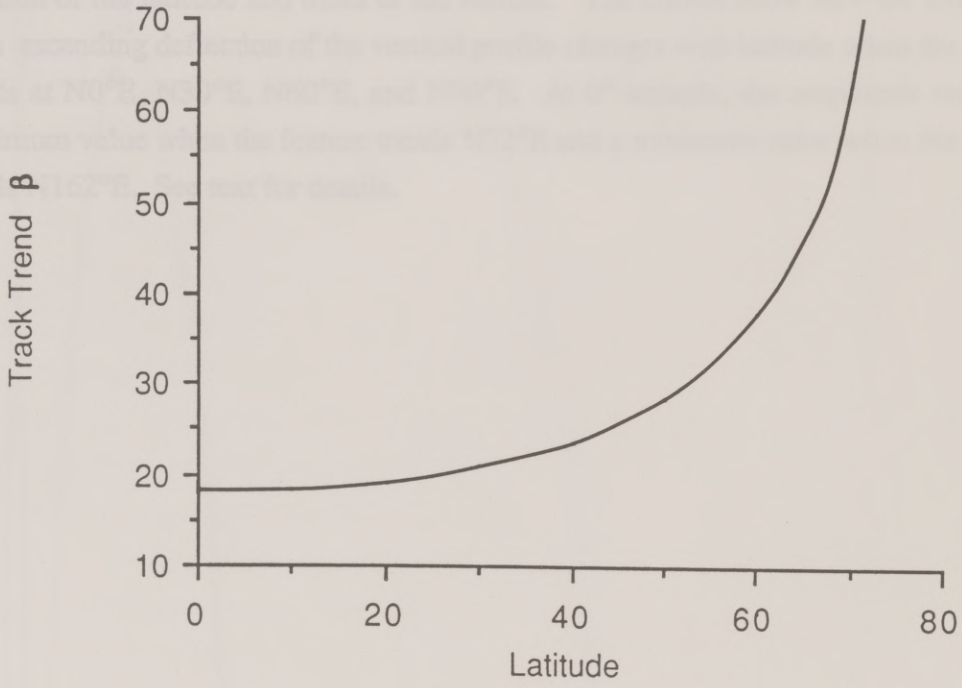
Track Trend β
70
60
50
40
30
20
10
0
20
40
60
80
Latitude

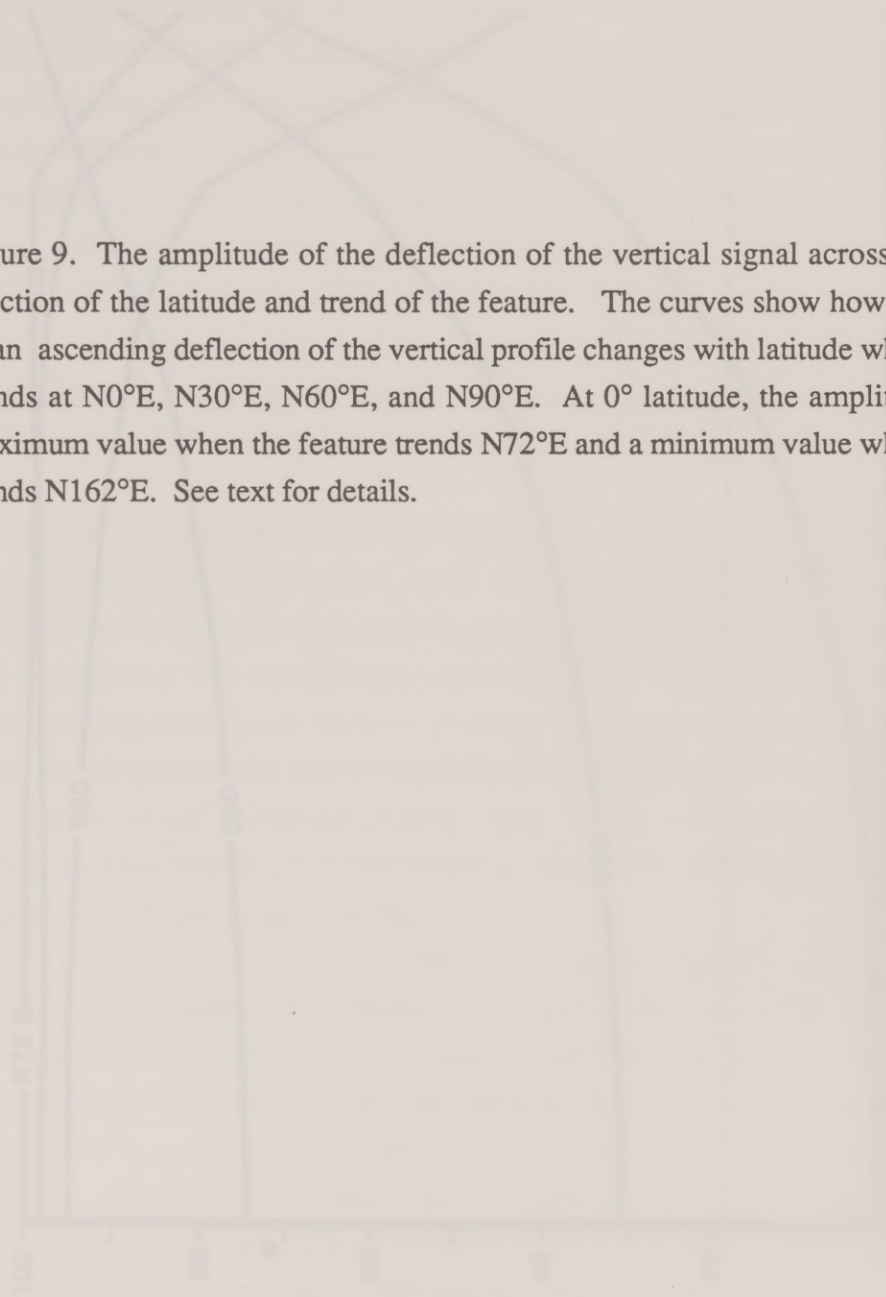

Figure 9. The amplitude of the deflection of the vertical signal across a feature is a function of the latitude and trend of the feature. The curves show how the amplitude of an ascending deflection of the vertical profile changes with latitude when the feature trends at N0°E, N30°E, N60°E, and N90°E. At 0° latitude, the amplitude reaches a maximum value when the feature trends N72°E and a minimum value when the feature trends N162°E. See text for details.

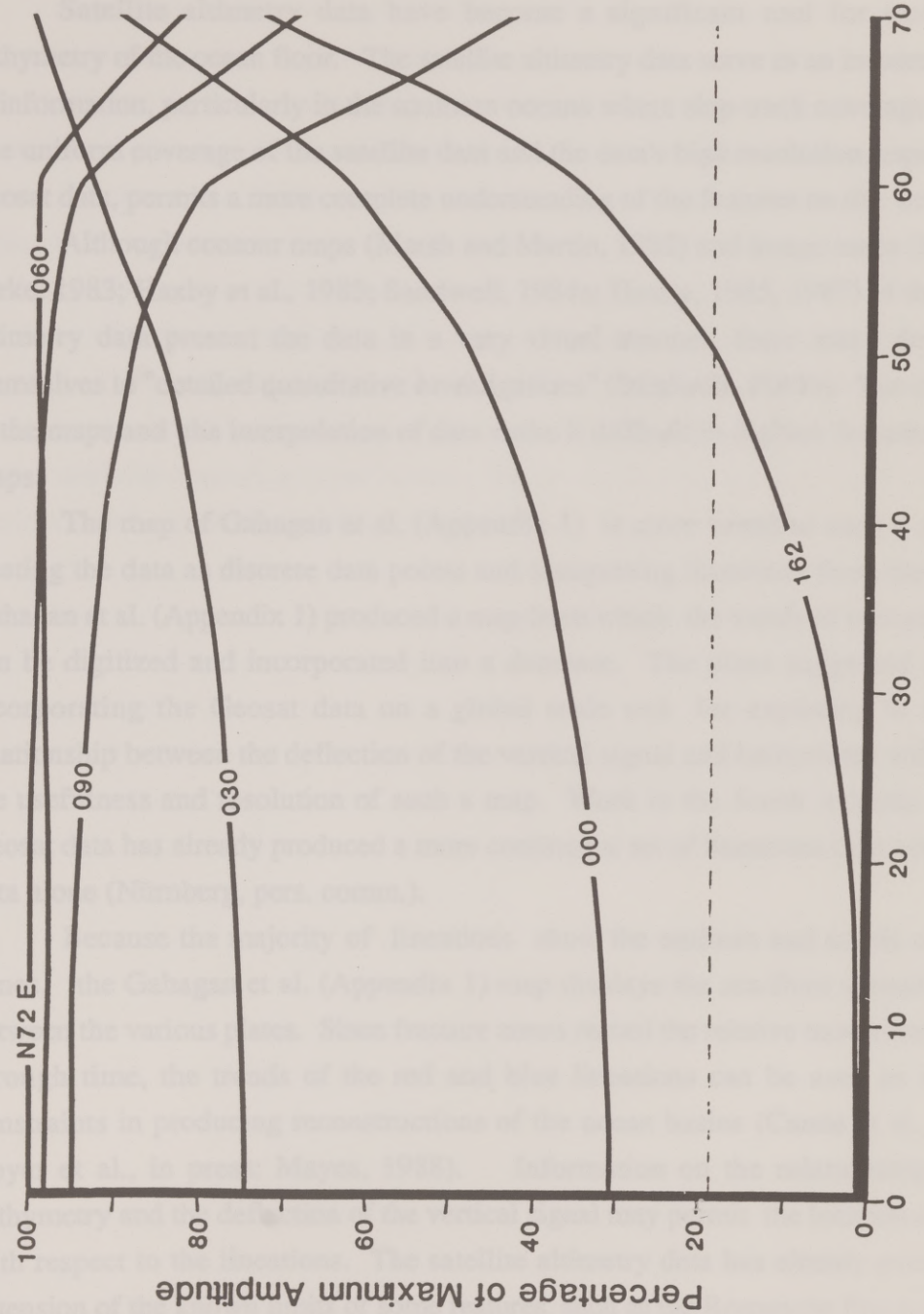
N72 E
060
090
030
000
162
100
80
60
40
20
0
0
10
20
30
40
50
60
70
Latitude (degrees)
Percentage of Maximum Amplitude

III. Conclusion

Satellite altimetry data have become a significant tool for studying the bathymetry of the ocean floor. The satellite altimetry data serve as an important source of information, particularly in the southern oceans where ship-track coverage is sparse. The uniform coverage of the satellite data and the data's high resolution, especially the Geosat data, permits a more complete understanding of the features on the ocean floor.

Although contour maps (Marsh and Martin, 1982) and image maps (Dixon and Parke, 1983; Haxby et al., 1983; Sandwell, 1984a; Haxby, 1985, 1987) of the satellite altimetry data present the data in a very visual manner, these maps do not lend themselves to "detailed quantitative investigations" (Sandwell, 1984b). The small scale of the maps and the interpolation of data make it difficult to digitize features from the maps.

The map of Gahagan et al. (Appendix 1) is more suited to such a study. By treating the data as discrete data points and interpreting lineations from these points, Gahagan et al. (Appendix 1) produced a map from which the trends of tectonic features can be digitized and incorporated into a database. The plans suggested above for incorporating the Geosat data on a global scale and for exploring in detail the relationship between the deflection of the vertical signal and bathymetry will increase the usefulness and resolution of such a map. Work in the South Atlantic using the Geosat data has already produced a more continuous set of lineations than using Seasat data alone (Nürnberg, pers. comm.).

Because the majority of lineations show the outlines and trends of fracture zones, the Gahagan et al. (Appendix 1) map displays the sea-floor spreading fabric between the various plates. Since fracture zones record the relative movement of plates through time, the trends of the red and blue lineations can be used as additional constraints in producing reconstructions of the ocean basins (Cande et al., in press; Royer et al., in press; Mayes, 1988). Information on the relationship between bathymetry and the deflection of the vertical signal may permit the location of features with respect to the lineations. The satellite altimetry data has already permitted the extension of the known limits of some features, such as the Romanche Fracture Zone in

the South Atlantic and the Tharp Fracture Zone in the South Pacific (Gahagan et al., Appendix 1).

Future work will combine Geosat satellite altimetry data with bathymetric and magnetic anomaly data to produce a tectonic chart of oceanic features. Because this tectonic chart may help to constrain the plate reconstruction models, the chart will be incorporated into a global isochron chart describing the tectonic history of the ocean basins. Larson et al. (1985) partially incorporated the Seasat altimetry data into some areas of their isochron chart. A recent attempt at using the Larson et al. (1985) isochrons to produce reconstructions of the ocean basins has, however, shown problems with the isochron chart and a general lack of self-consistency (Scotese et al., in press). The incorporation of the satellite altimetry data into a new isochron chart on a global basis should help produce a high resolution isochron chart which is consistent with a seafloor-spreading plate model. Future work will use this isochron chart to produce depth-age studies of the ocean basins.

IV. Appendix 1

Tectonic fabric map of the ocean basins from satellite altimetry data[1]

Abstract

Satellite altimetry data provides a new source of information on the bathymetry of the ocean floor. The tectonic fabric of the oceans (i.e. the arrangement of fracture zones, ridges, volcanic plateaus and trenches) is revealed by changes in the horizontal gravity as recorded by satellite altimetry measurements. Seasat and Geosat altimetry data have been analyzed and a global map of the horizontal gravity has been produced that can be used to identify a variety of marine tectonic features. The uniformity of the satellite coverage provides greater resolution and continuity than maps based solely on ship-track data. This map is also the first global map to incorporate the results of the Geosat mission, and as a result, new tectonic features are revealed at high southerly latitudes.

This map permits the extension of many tectonic features well beyond what was previously known. For instance, various fracture zones, such as the Ascension, Tasman, and Udintsev fracture zones, can be extended much closer to adjacent continental margins. The tectonic fabric map also reveals many features that have not been not previously mapped. These features include extinct ridges, minor fracture zone lineations, and seamounts. In several areas, especially across aseismic plateaus or along the margins of the continents, the map displays broad gravity anomalies whose origin may be related to basement structures.

---

[1] A revised version of Appendix 1 has been submitted to Tectonophysics under the title "Tectonic fabric map of the ocean basins from satellite altimetry data" by L.M. Gahagan, C.R. Scotese, J.Y. Royer, D.T. Sandwell, J.K. Winn, R.L. Tomlins, M.I. Ross, J.S. Newman, R.D. Müller, C.L. Mayes, L.A. Lawver, and C.E. Heubeck.

Introduction

During the past decade, remote sensing data obtained from orbiting satellites has provided new information about geology at the Earth's surface (LANDSAT) and the structure of the Earth's magnetic (MAGSAT) and gravity fields (Seasat and Geosat). The geoid is an equipotential gravitational surface that is closely approximated by the sea surface. The shape of the geoid and sea surface change in response to gravitational anomalies within the earth. The long-wavelength signals (>1000 km) of the geoid are due to structures deep within the Earth while the short-wavelength signals (~200 km or less) are the result of mass excesses and deficits near the surface of the Earth. In areas of excess mass, such as in the vicinity of an oceanic ridge or seamount, there are distinct geoid highs; in areas where there are mass deficits, such as trenches or deep fracture zone valleys, there are corresponding geoid lows. This direct correlation between the short-wavelength features (or high-frequency component) of the geoid and the bathymetry of the ocean floor (Haxby et al., 1983; Sandwell, 1984a) has been successfully used to identify and locate a variety of bathymetric features. Geoid data, as collected by satellite, has yielded information on trenches (McAdoo, 1981), on the location of fracture zones in the Pacific (Sailor and Okal, 1983) and Atlantic (Cande et al., in press) oceans, and on the global dispersement of seamounts (Craig and Sandwell, in press).

In this paper we present a global map (Plate 1), based on measurements of the high-frequency component of the geoid, that defines the trends and outlines of tectonic features on the ocean floor. This map can be used to identify oceanic fracture zones, active and extinct spreading ridges, seamounts, trenches, and aseismic volcanic edifices, as well as some of the aspects of the structure of deeply buried basement features along rifted continental margins. The lineations on the map that correspond to fracture zones record the movement of the plates through time and thus serve as tectonic 'flowlines' between the plates. These flowlines, together with the other features on the map, reveal how the tectonic history of the ocean basins has been woven into the ocean floor itself, and thus reveal what we refer to as the 'tectonic fabric' of the ocean basins.

Plate 1. This map displays the tectonic fabric of the ocean basins determined by satellite (Seasat and Geosat) altimetry data. The map should be 'read' from south to north. The blue lineations represent positive gravity gradients (or slopes in the sea surface), and the red lineations represent negative gravity gradients. For instance, crossing a blue lineation is equivalent to going 'upslope' and crossing a red lineation is equivalent to going 'downslope.' Although the tectonic fabric map is dominated by linear flowlines corresponding mostly to fracture zones, other tectonic features, such as ridges and aseismic plateaus, can be identified.

Our results, though similar to the work of Haxby (1985, 1987), were obtained by a different technique. Rather than work with gridded, areal averages (Haxby, 1985, 1987), our interpretation is based on a direct analysis of individual measurements. By working with discrete data points, we have been able to increase the resolution of our interpretations and map previously unknown tectonic features, as well as resolve the shape of known tectonic features in greater detail.

In the following sections we outline the methods that we have used to analyze the satellite altimetry data. This includes a brief discussion of the processing of the satellite altimetry data as well as the techniques that were used to produce the maps (Plate 1). In the first part of the discussion section, guidelines are given that enable the reader to identify the distinctive geoid signals that accompany ridges, trenches, fractures zones, etc. In the second part of the discussion section, some of the major tectonic features that we have mapped are described. This section includes a discussion of the correlation between our interpretations and known bathymetric features, as well as a description of some of the previously unmapped, tectonic features that have been revealed by satellite altimetry data. In the conclusion, we discuss how the tectonic fabric map of the ocean basins is being used to produce plate reconstructions and how it might be used to provide insights into the kinematics of the plate tectonic process.

Methods

Seasat and Geosat Missions

In June, 1978, NASA launched the Seasat satellite to collect data which would provide information on oceanic parameters such as the height of the sea surface, wave height and sea-surface winds (Lame and Born, 1982). While ground-tracking lasers located the satellite in its orbit, the satellite used a radar altimeter to measure the altitude between itself and the sea surface, h (Figure 1). After instrument, atmospheric and geophysical corrections were made to h, this distance was subtracted from the distance between the satellite and a reference ellipsoid for the Earth (h*). The difference between h* and h is the height of the sea surface (h_g) (Figure 1).

During its three months of operation, the Seasat satellite collected more than four million data points (Sandwell, 1984b). The satellite, possessing a footprint of 2-5 km in diameter, made altimetry measurements 10 times per second. These were averaged into one point per second. The Seasat satellite obtained several global data sets with a 165 km equatorial spacing of ground tracks and a three-day repeat-orbit set with a 900 km equatorial spacing of ground tracks (Tapley et al., 1982). Data was collected along both ascending orbital tracks (trending southeast to northwest) and descending orbital tracks (trending northeast to southwest).

In order to assure the accuracy of the Seasat data, the Jet Propulsion Laboratory, in conjunction with NASA, formed the Seasat Altimeter/Precision Orbit Determination Experiment Team. Using correction algorithms (Lorell, 1980; Parke et al., 1980; Hancock et al., 1980) and in situ surface gravity measurements the team was able to verify the accuracy and resolution of the Seasat measurements (Tapley et al., 1982; Lame and Born, 1982). Corrections were made for instrumentation, orbit, temporal variations and other secular effects. Among its conclusions, the team was able to determine that the altimetry measurements between the satellite and sea surface were accurate to within 10 cm for wave heights of less than 20 m as determined by the satellite (Tapley et al., 1982).

On March 12, 1985, the geodesy satellite, or Geosat was launched by the U.S. Navy in order to complete Seasat mission and obtain a high resolution, global-scale, oceanographic data set. John Hopkins Applied Physics Laboratory (APL) constructed

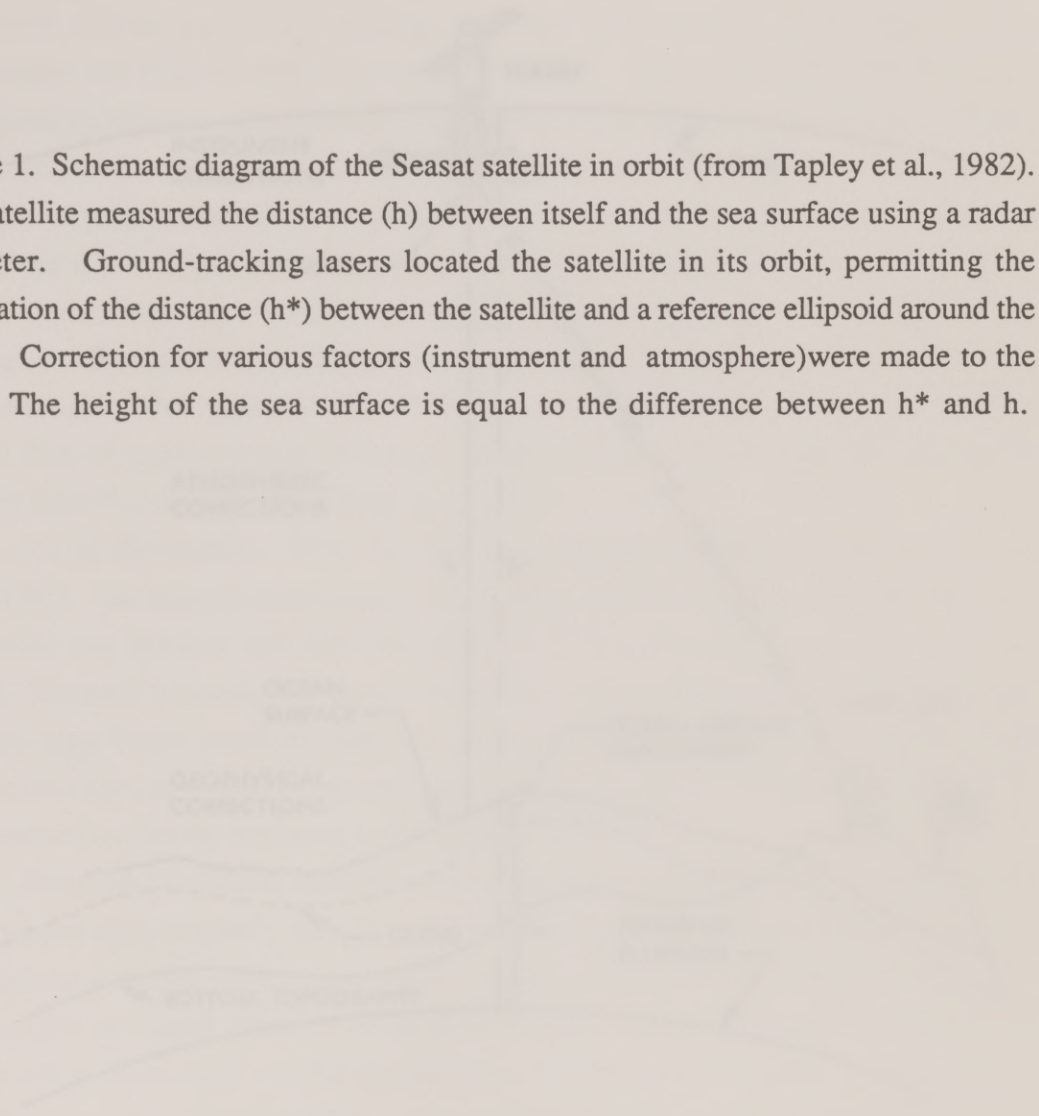

Figure 1. Schematic diagram of the Seasat satellite in orbit (from Tapley et al., 1982). The satellite measured the distance (h) between itself and the sea surface using a radar altimeter. Ground-tracking lasers located the satellite in its orbit, permitting the calculation of the distance (h*) between the satellite and a reference ellipsoid around the Earth. Correction for various factors (instrument and atmosphere)were made to the data. The height of the sea surface is equal to the difference between h* and h.

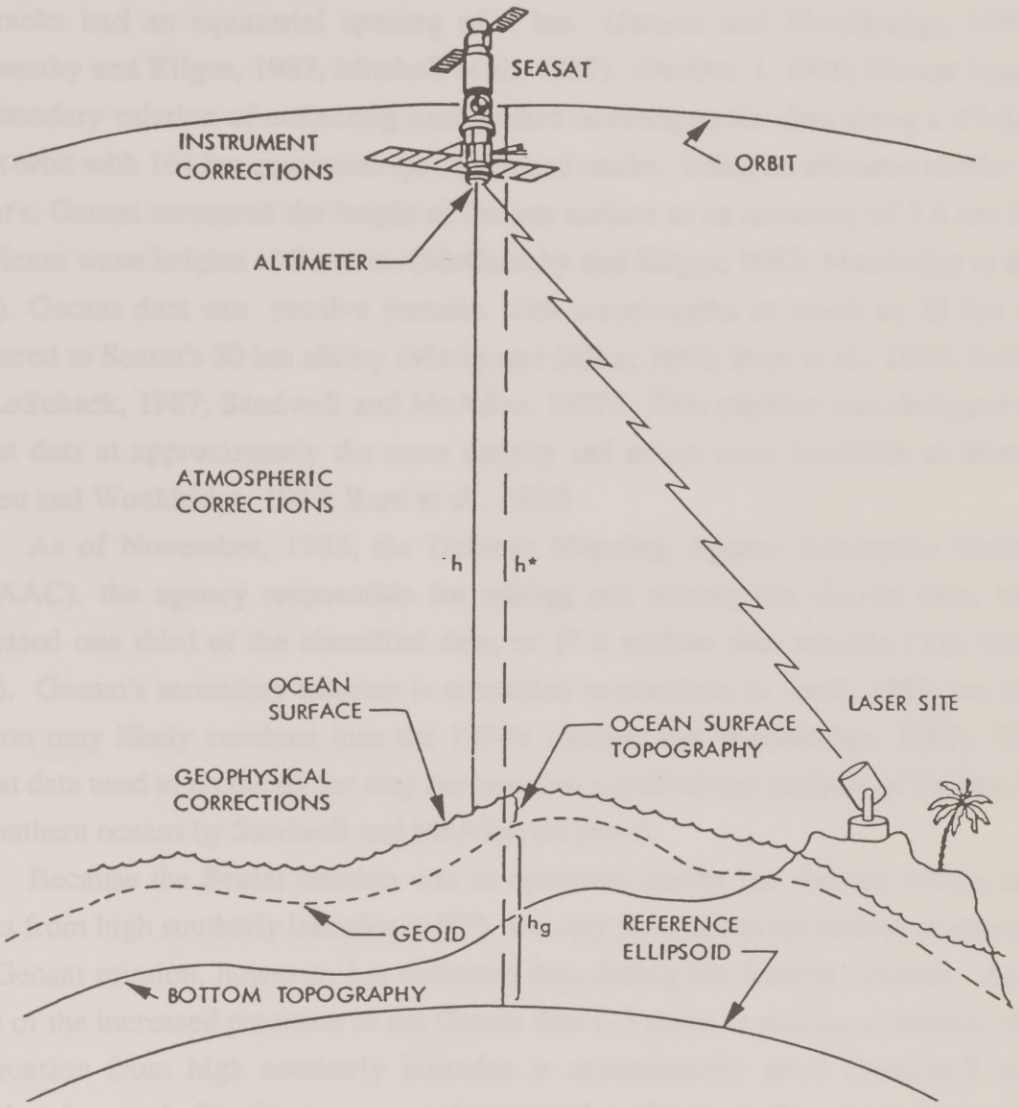
SEASAT
INSTRUMENT CORRECTIONS
ORBIT
ALTIMETER
ATMOSPHERIC CORRECTIONS
h
h*
OCEAN SURFACE
OCEAN SURFACE TOPOGRAPHY
LASER SITE
GEOPHYSICAL CORRECTIONS
GEOID
hg
REFERENCE ELLIPSOID
BOTTOM TOPOGRAPHY

the satellite and is responsible for its operation (Mitchell et al., 1987). During its 18-month, primary mission, Geosat made over 270 million observations along an orbital track of 200 million kilometers. The orbits repeated approximately every three days and the tracks had an equatorial spacing of 4 km (Jensen and Wooldridge, 1987; McConathy and Kilgus, 1987, Mitchell et al., 1987). On Oct. 1, 1986, Geosat began its secondary mission of collecting unclassified oceanographic data along a 17-day repeat orbit with 164 km equatorial-spaced ground tracks. Using an altimeter similar to Seasat's, Geosat measured the height of the sea surface to an accuracy of 3.5 cm for significant wave heights of 2 meters (McConathy and Kilgus, 1987; MacArthur et al., 1987). Geosat data can resolve features with wavelengths as small as 32 km as compared to Seasat's 50 km ability (Marks and Sailor, 1986; Born et al., 1987; Sailor and LeSchack, 1987; Sandwell and McAdoo, 1987). This mission was designed to collect data at approximately the same density and at the same locations as Seasat (Jensen and Wooldridge, 1987; Born et al., 1987).

As of November, 1986, the Defense Mapping Agency Aerospace Center (DMAAC), the agency responsible for editing and storing the Geosat data, had processed one third of the classified data, or 17.2 million data records (Van Hee, 1987). Geosat's secondary mission is scheduled to conclude in April, 1989, but the mission may likely continue into the 1990's (Jensen and Wooldridge, 1987). The Geosat data used to produced our map are based on a preliminary analysis of the data in the southern oceans by Sandwell and McAdoo (in press).

Because the Seasat mission was in operation during the Austral winter, the results from high southerly latitudes (>60°) are very poor due to the effects of sea ice. The Geosat mission, however, has collected data during the Austral summer. As a result of the increased precision of the Geosat data (~3 times as precise as Seasat), the information from high southerly latitudes is exceptionally good (Sandwell and McAdoo, in press). For this reason, our interpretation of tectonic features between 55° and 72° S are based on Geosat altimetry data; all other tectonic features are based on Seasat data.

Deflection of the Vertical and Signal Filtering

In order to emphasize the subtle variations in the sea surface, the slope of the sea surface (deflection of the vertical) was used to map the tectonic fabric of the ocean floor. The deflection of the vertical signal is the angle, in microradians, between the line connecting the satellite and the sea surface, and the line normal to the sea surface. In essence, it is the first derivative of the sea surface. Taking the first derivative of the altimetry signal, however, tended to increase the short-wavelength noise (Figure 2a).

To eliminate the short-wavelength noise, we convolved a Gaussian-shaped filter ($\exp[-t^2/2\sigma^2]$; $\sigma = 1$ second) with each profile as given by the following equation:

$$S(t_o) = \frac{\sum_{n=0}^{L} S_n e^{-\left(\frac{(t_n - t_o)^2}{2\sigma^2}\right)}}{\sum_{n=0}^{L} e^{-\left(\frac{(t_n - t_o)^2}{2\sigma^2}\right)}}$$

where S = geoid slope in the deflection of the vertical (DV) signal
t = distance in seconds along the track of the DV signal
σ = half-width of the filter
$L = 3 \cdot \sigma$

The satellite has a ground velocity of 6.6 km/sec so this filter removes wavelengths less than 19.8 km (a distance equal to the spacing of three consecutive altimetry measurements). This resulted in a considerably smoother signal with well-defined peaks and troughs (Figure 2b). After the short-wavelength noise was eliminated, the next step was to remove the broad, long-wavelength features of the geoid associated with deep-seated gravity anomalies and thermal convection. To remove the long-wavelength component of the signal, we used the same filter with a half-width of 10 seconds, that eliminated features with wavelengths shorter than 200 km. The filtered profile was then subtracted from the original profile. The resulting band-pass filtered

Figure 2. The processing steps performed on the data. (a) An unfiltered deflection of the vertical profile. (b) A low-pass Gaussian filter removed wavelengths less than 19.8 km to decrease the short wavelength noise. (c) A high-pass Gaussian filter removed wavelengths greater than approx. 200 km. (d) The positions of the peaks, troughs and zero crossings (inflection points) were recorded and symbolically represented by circles, triangles and crosses, respectively, which were scaled according to the amplitude of the signal. Only those peaks and troughs with amplitudes greater than the 7.5 microradians threshold were retained.

a
b
c
p

signal (Figure 2c), though similar in shape to the previous one, is more symmetrically disposed about the baseline. In Figure 3, the band-pass filtered deflection of the vertical profile is plotted along ascending satellite tracks in the Northeast Pacific; the locations of the Mendocino and Pioneer fracture zones can be clearly seen.

Map Preparation

In order to produce the tectonic fabric map (Plate 1), the peaks and troughs of the deflection of the vertical signal were "picked", i.e. represented by discrete symbols (Figure 2d). As illustrated in Figure 2d, circles represent peaks (positive slopes in the sea surface), and triangles represent troughs (negative slopes in the sea surface). The symbols were scaled in proportion to the absolute magnitude of the amplitude of the signal (in microradians). The x's and plus signs represent the location where the signal crosses the zero line (inflection point). The x's were scaled by using the absolute magnitude of the amplitude of the previous peak or trough. These symbols were then connected by hand to form linear features (Figure 4). As illustrated in Figure 4, this technique allowed us to plot data from both the ascending and descending satellite paths simultaneously, without crowding or confusion. Figure 5 illustrates the authorship responsibilities for the interpretations of the tectonic fabric (Plate 1).

The satellite altimetry picks were generated by converting the amplitudes of the signals from meters/second to microradians using the following equations:

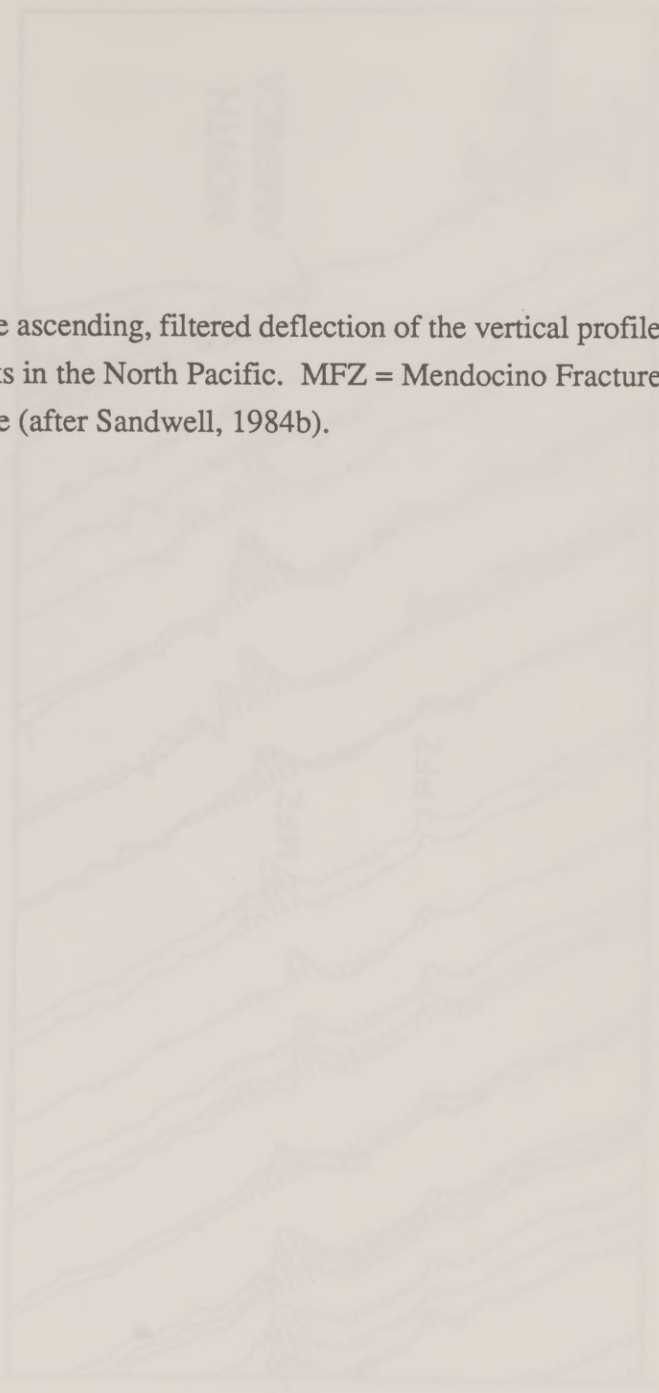

Figure 3. The ascending, filtered deflection of the vertical profiles are plotted along the satellite tracks in the North Pacific. MFZ = Mendocino Fracture Zone; PFZ = Pioneer Fracture Zone (after Sandwell, 1984b).

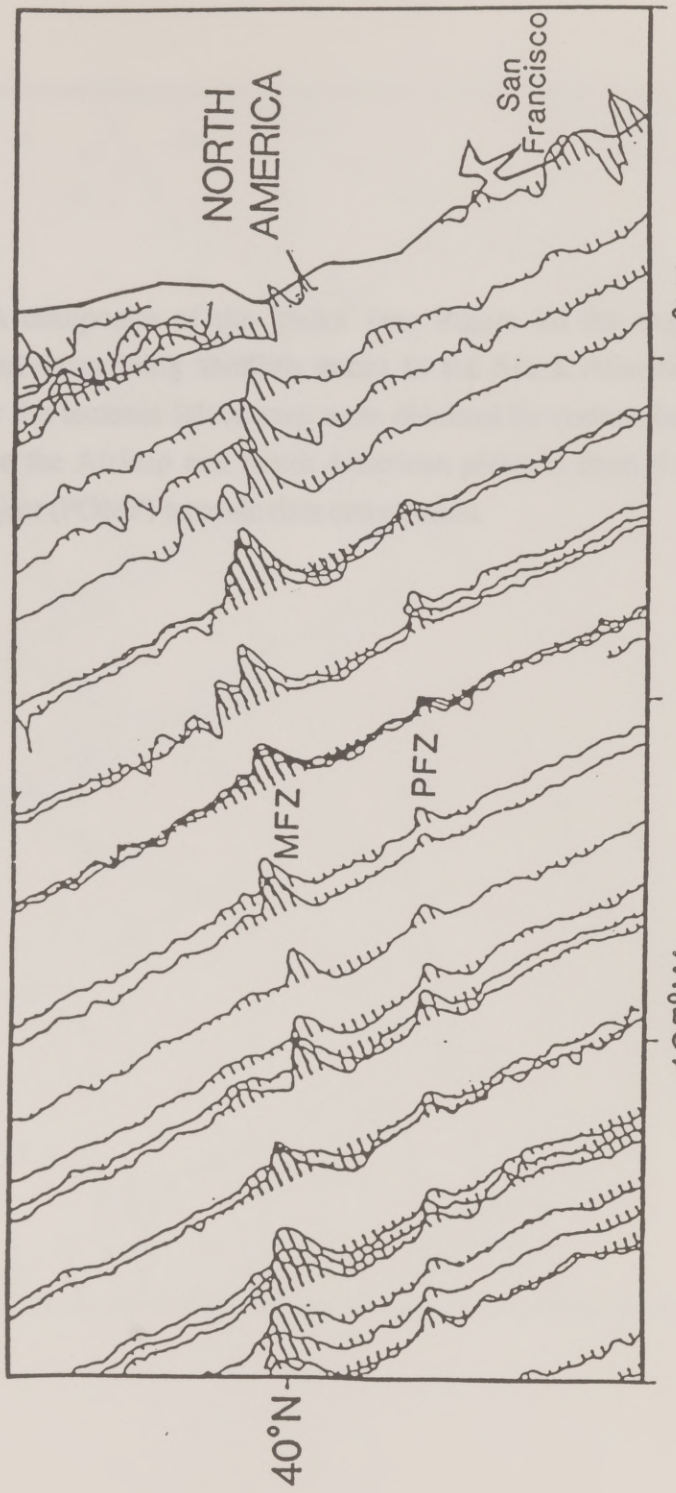
NORTH
AMERICA
San
Francisco
MFZ
PFZ
40°N
-135°W
-125°W

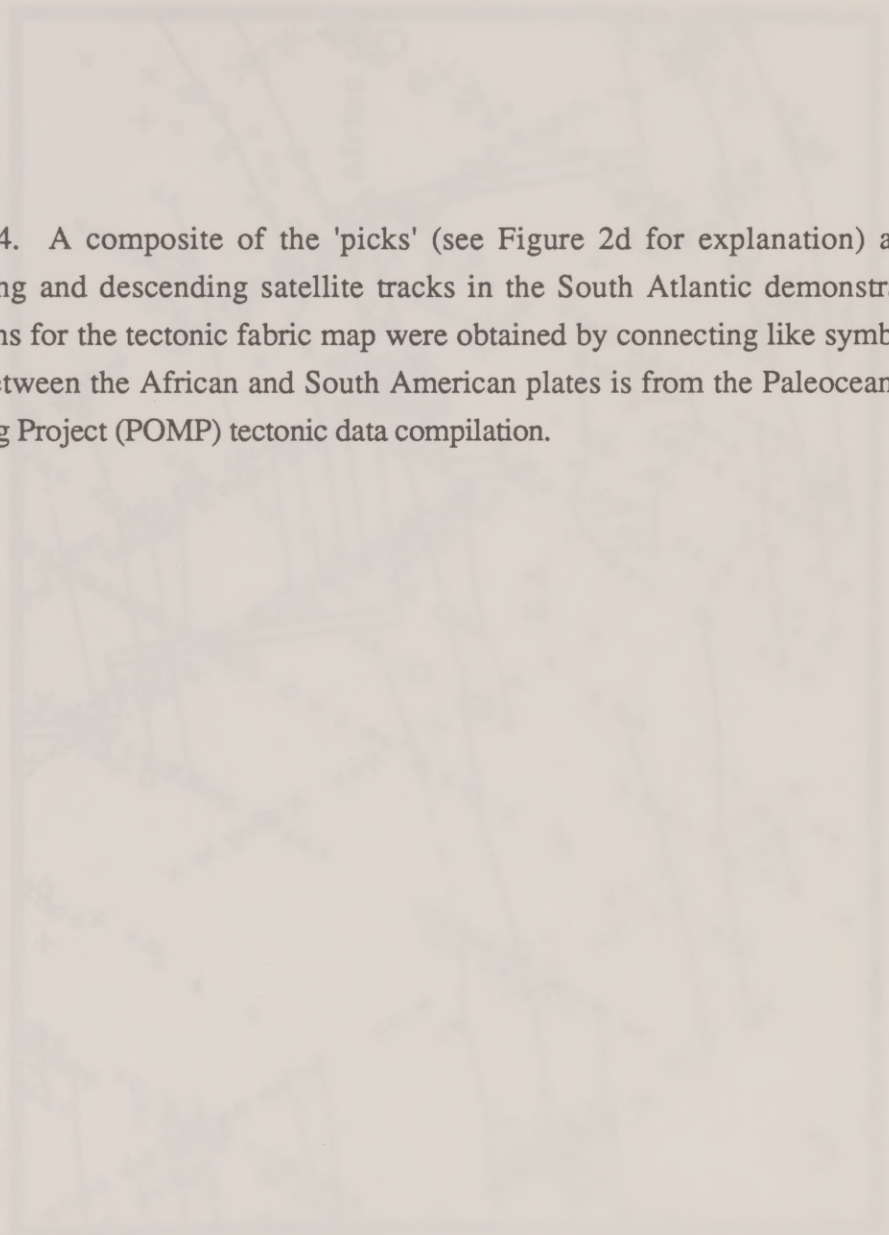

Figure 4. A composite of the 'picks' (see Figure 2d for explanation) along the ascending and descending satellite tracks in the South Atlantic demonstrates how lineations for the tectonic fabric map were obtained by connecting like symbols. The ridge between the African and South American plates is from the Paleoceanographic Mapping Project (POMP) tectonic data compilation.

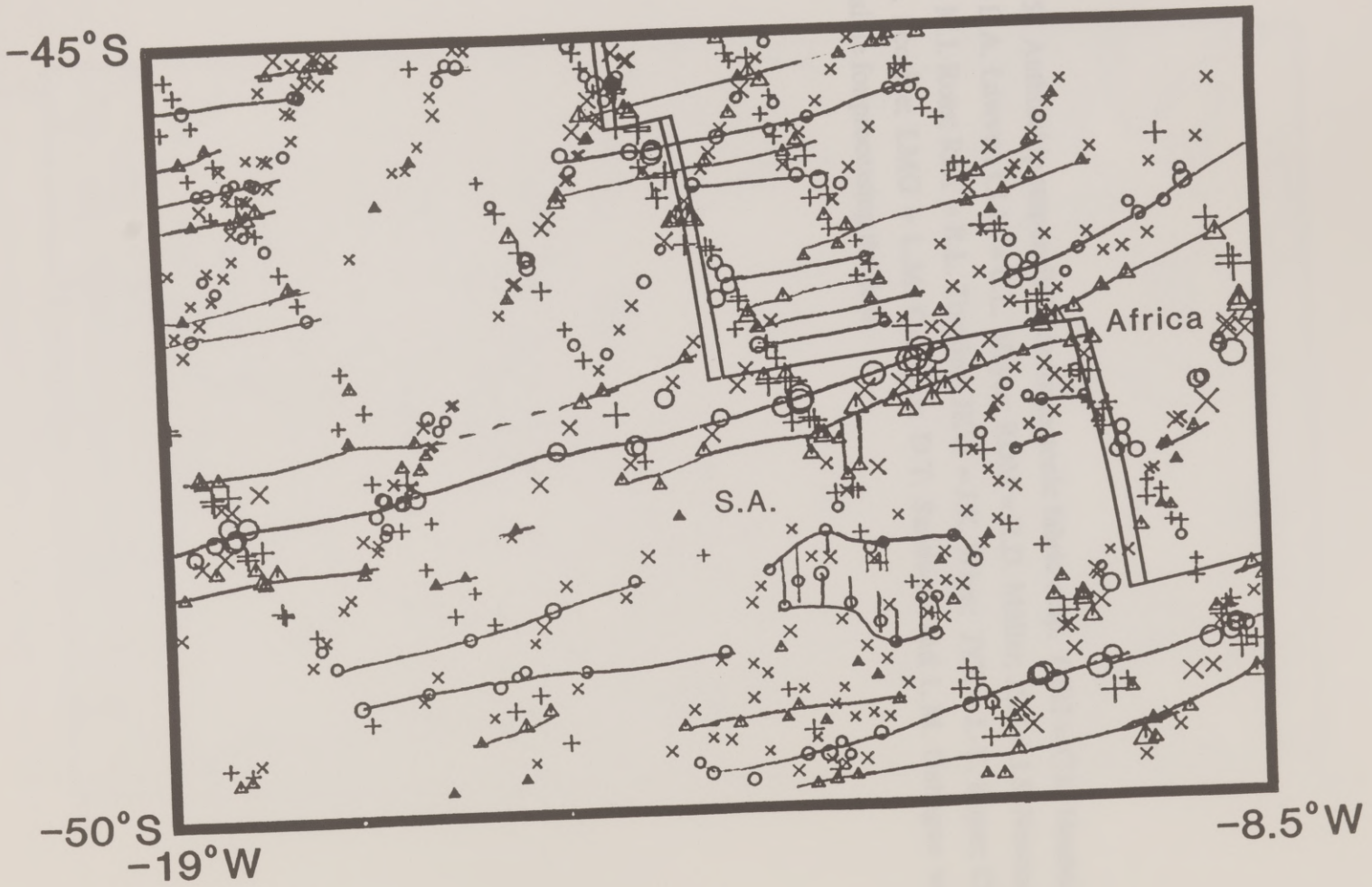
-45°S
Africa
S.A.
-50°S
-19°W
-8.5°W

Figure 5. Authorship responsibilities for tectonic fabric map. CEH = C.E. Heubeck; LAL = L.A. Lawver; CLM = C.L. Mayes; RDM = R.D. Müller; JSN = J.S. Newman; MIR = M.I. Ross; RLT = R.L. Tomlins; JKW = J.K. Winn; JYR = J.-Y. Royer; CRS = C.R. Scotese; LMG = L.M. Gahagan; D.T. Sandwell and L.M. Gahagan were responsible for processing the data.

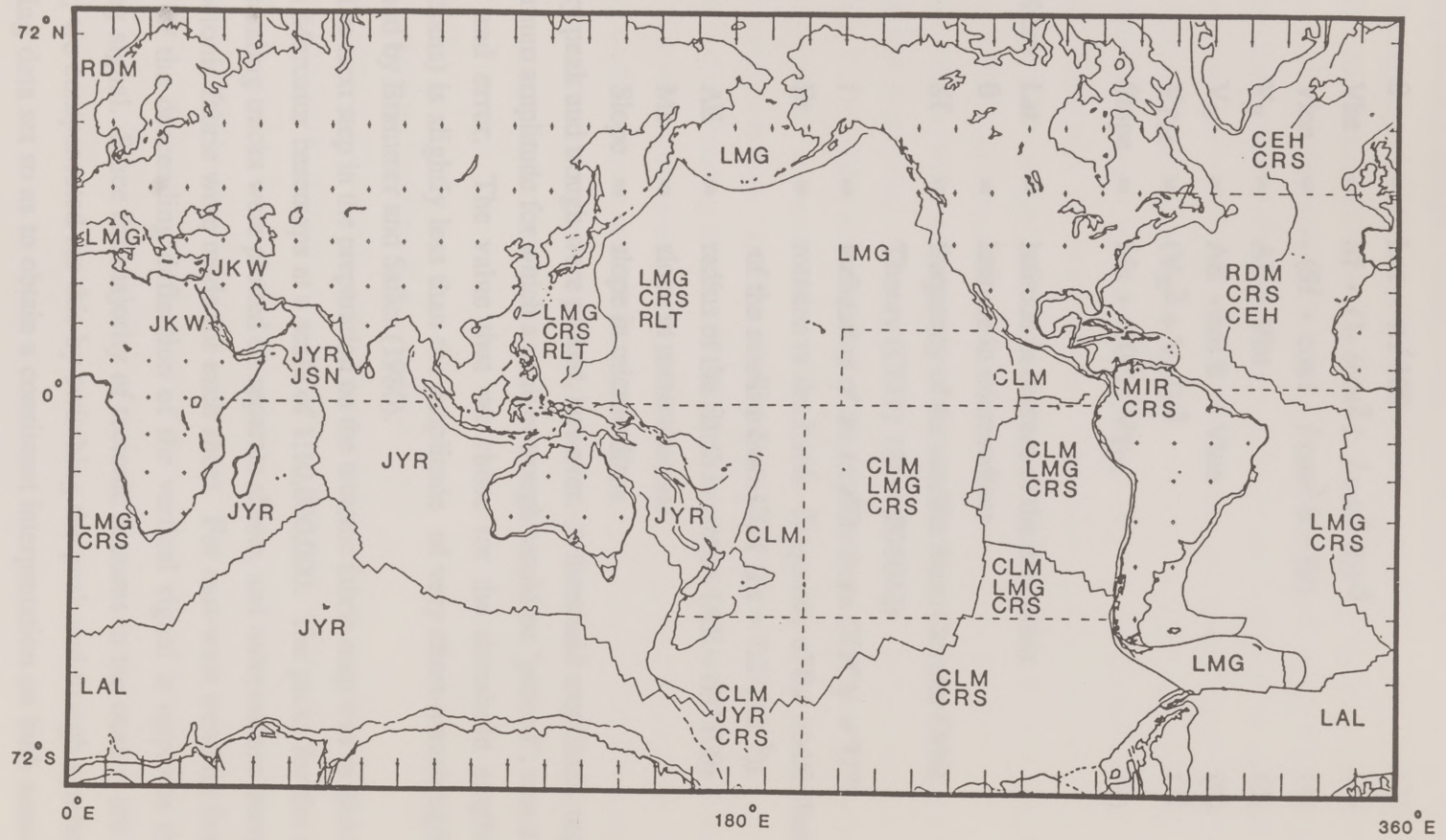
72°N
0°
72°S
0°E
180°E
360°E
RDM
LMG
LMG
JKW
JKW
JYR
JSN
LMG
CRS
RLT
LMG
CRS
RLT
LMG
LMG
CEH
CRS
RDM
CRS
CEH
CLM
MIR
CRS
CLM
LMG
CRS
JYR
JYR
JYR
CLM
CLM
LMG
CRS
LMG
CRS
CLM
LMG
CRS
JYR
LAL
CLM
JYR
CRS
CLM
CRS
LMG
LAL

$$\theta = Lat \cdot \pi / 180 \quad (2)$$

$$Vlat = Sf \cdot (1 - (\cos^2 i \ / \cos^2 \theta))^{.5} \quad (3)$$

$$Vlon = -(Sf \cdot \cos i \ / \cos^2 \theta + Er) \quad (4)$$

$$V_y = AE \cdot Vlat \quad (5)$$

$$V_x = AE \cdot \cos \theta \cdot Vlon \quad (6)$$

$$V_{Tot} = (V_x^2 + V_y^2)^{.5} \quad (7)$$

$$Slope = Ms \cdot (10^6) / V_{Tot} \quad (8)$$

where Lat = latitude in degrees of the data point

θ = latitude in microradians

Sf = frequency of the satellite from Circular Orbit Theory (COT) (Sf = .001042)

i = inclination of the satellite from COT (i = 72°)

Er = rotation of the Earth - frequency of the nodal plane of the satellite from COT (Er = $7.27(10^{-5})$)

AE = radius of the Earth in meters (AE = 637100)

Ms = slope in meters/second

Slope = slope in microradians

Not every peak and trough were picked, however. A threshold amplitude, representing the minimum amplitude for which a peak or trough would be "picked", was determined by trial and error. The value that we chose for the threshold amplitude (7.5 microradians) is slightly less than the amplitude of very short-wavelength noise as determined by Brammer and Sailor (1980).

The next step in the preparation on the tectonic fabric map was to plot the Seasat picks on Mercator basemaps at a scale of 1:10,000,000. The picks for the ascending and descending tracks were plotted on separate sheets, and independent interpretations of the tectonic fabric were made for each sheet. For east-west trending features, the polarity of the descending deflection of the vertical signal is opposite that of the ascending signal. Since the majority of tectonic features in the oceans are east-west trending, we compensated for this by switching the peak and trough symbols for the descending data set so as to obtain a consistent interpretation on both ascending and

descending sheets (Gahagan, 1988). Using knowledge of the spreading history of the area, the interpreter began drawing lineations by connecting like symbols by hand. A 'lineation' consists of three or more like symbols trending in the same direction with less than ~1.5° latitude between the individual symbols. A 'major feature' consists of six or more like symbols along trend. If a symbol was 2° latitude or less from a major feature but was obviously part of that feature, then the symbol was connected to the feature. If two like symbols were trending in the same direction as the other lineations in the immediate area, they were considered part of the overall fabric and were connected. Typically, the interpretation of the tectonic fabric would begin with the identification of the major features. The identification of these features provided a framework from which more speculative interpretations could be made.

After these preliminary interpretations were made, the interpretations from the ascending and descending sheets were superimposed and a final composite map was made (Plate 1). By independently interpreting the tectonic fabric for the ascending and descending tracks, we could confidently differentiate between actual features and spurious interpretations. In this case, actual features would appear on both the ascending and descending maps, whereas spurious features were less consistent. In all cases, by combining the interpretations from the ascending and descending tracks we were able to draw more consistent and continuous features. The last stage in map interpretation was to compare the interpreted tectonic features with bathymetric data (GEBCO maps) in order to delete obvious errors and misinterpretations.

Discussion

Map Interpretation: Reading the Red and Blue Lines

A variety of tectonic features, including: fracture zones, spreading axes, seamounts, aseismic plateaus and trenches, can be identified from the lineations illustrated on Plate 1. In the following section we provide guidelines for identifying these tectonic features and delineating their boundaries. It has been our experience that when detailed comparisons of the tectonic fabric map and bathymetric maps are made, there is excellent agreement between the location of known features and our predictions from satellite altimetry.

We color-coded the lineations we obtained by connecting the picks, using blue for lines through peaks (circles) and red for lines through troughs (triangles). The red and blue lines can be regarded in a variety of ways. Essentially, they represent positive (blue) and negative (red) slopes of the sea surface. Because the slope in the sea surface is directly related to the horizontal component of the gravity field, the blue and red lines are the positive (blue) and negative (red) horizontal gravity anomalies. As discussed earlier, the gravity anomalies are due primarily to the topography of the sea floor (fracture zones, trenches, etc.) and, as a consequence, the red and blue lines can also be thought of as lines along the maximum slopes of these submarine features. For instance, a blue line indicates an "upslope" direction, and, conversely, a red line means a "downslope" direction. For instance, in the case of a fracture zone, a red line indicates that the satellite crossed from younger crust over to older crust, going from high ground down to low ground, in accordance with the depth/age step.

The tectonic fabric on our map is not only constructed from red and blue lineations but also from red and blue hatchured zones. These zones are the result of broad, uneven or 'rough' gravity surfaces that cause several peaks (or troughs) to occur together instead of one maximum peak (or trough) (Figure 2c-d). The lines forming the hatchuring were drawn through one or more symbols and do not correspond to the number of symbols present. These broad zones of positive (blue) and negative (red) slope occur both over oceanic crust and over continental crust along the continental margins. These hatchured zones may be due to 1) the expression of bathymetric features (e.g. the Rio Grande and Walvis Ridges) or basement structures (e.g. the Colorado and Salado basins), 2) the presence of volcanism associated with hot spots or "leaky transforms," 3) areas of compression and extension along fracture zones, or 4) some deeper unknown cause.

Because the blue and red lines represent slopes (gradients), there is one additional ambiguity. Which way is up? The slope is a vector that has both a magnitude and a direction. To interpret the map, one must "read" the map from south to north. In this manner, a blue line indicates that the slope is increasing from south to north (upslope); conversely a red line indicates that the slope is decreasing from south to north (downslope). A ridge would have a blue line (upslope) along its southern edge, and a red line (downslope) along its northern edge. A trench or valley, would

have the opposite pattern, i.e. a red line (downslope) along its southern edge and blue line (upslope) along its northern edge. The meaning of the blue and red lines can be best understood by referring to the colors associated with the continental margins in Plate 1. All south-facing continental margins are marked by blue lines (upslope), while all north-facing margins are marked by red lines (downslope). It must be remembered that the blue and red lines do not correspond to the tectonic features, themselves, but rather the colored lines indicate the maximum slopes or gradients associated with these features.

The patterns of sea-surface slope associated with major tectonic features are generally straightforward; each tectonic feature has it own pattern. In the following section, we review the patterns in sea surface slope associated with fracture zones, seamounts, ridges, aseismic plateaus, continental margins, and trenches.

Fracture Zones

The long, linear features associated with fracture zones are the most distinctive features on Plate 1. However, these tectonic flowlines, which have recorded the movement of plates through time, do not correspond to the fracture zones on a one-to-one basis. The location of the fracture zone relative to the red and blue lines depends on: 1) the fracture zone's morphology, 2) the spreading rate of the adjacent ridge axis, and 3) the age offset across the fracture zone. In general, fracture zones with small age offsets (0 to 10 Ma) that were generated along ridges with slow spreading rates (< 4 cm/yr) are characterized by deep valleys (Figure 6a). These fracture zones are characterized by a positive anomaly and negative anomaly in the slope of the sea-surface (Figure 6a). In these cases, the fracture zone will lie between a pair of red and blue lines (Plate 1). The red line that is always located to the south of the blue line, indicates the downslope portion of the fracture zone valley; the blue line indicates the upslope portion of the fracture zone valley.

At the other end of the spectrum are those fracture zones like the Mendocino Fracture Zone that are characterized by large age offsets (>20 Ma) and that are associated with fast spreading ridges (> 10 cm/yr). Topographically, these fracture zones are characterized by large escarpments (Figure 6b). The sea-surface slope can be positive (Figure 6b) or negative depending on the whether the crust is younger to the

Figure 6. Within a particular spreading regime, fracture zones are characterized, to an extent, by particular bathymetric expressions that are reflected by the geoid. If the spreading rate and age offset along a fracture zone and the fracture zone's morphology are known, the deflection of the vertical profile can be used to locate the fracture zone. (a) A fracture zone associated with a slow spreading rate and a small age offset is characterized by a large trench and, as a result, is located at the inflection point of the deflection of the vertical profile. (b) A fracture zone associated with a fast spreading rate and a large age offset is characterized by a large escarpment and, as a result, is located at the peak of the deflection of the vertical profile (as the satellite travels across older to younger crust).

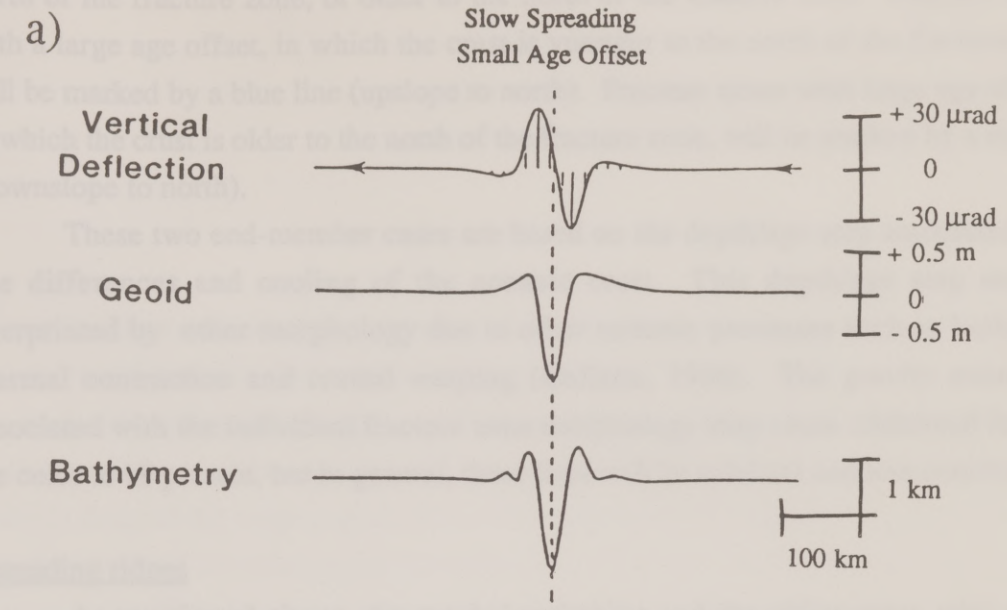
a)
Slow Spreading
Small Age Offset
Vertical Deflection
+ 30 µrad
0
- 30 µrad
Geoid
+ 0.5 m
0
- 0.5 m
Bathymetry
1 km
100 km
Fracture Zone

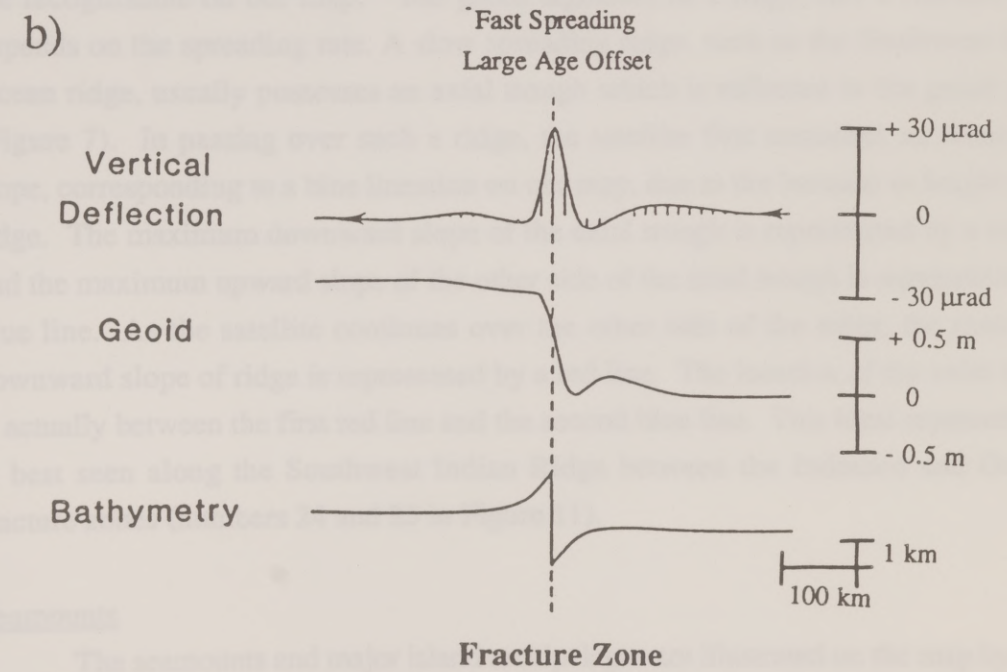
b)
Fast Spreading
Large Age Offset
Vertical Deflection
+ 30 µrad
0
- 30 µrad
Geoid
+ 0.5 m
0
- 0.5 m
Bathymetry
1 km
100 km
Fracture Zone

north of the fracture zone, or older to the north of the fracture zone. Fracture zones with a large age offset, in which the crust is younger to the north of the fracture zone will be marked by a blue line (upslope to north). Fracture zones with large age offsets, in which the crust is older to the north of the fracture zone, will be marked by a red line (downslope to north).

These two end-member cases are based on the depth/age step associated with age differences and cooling of the oceanic crust. This depth/age step may be overprinted by other morphology due to other tectonic processes such as horizontal thermal contraction and crustal warping (Collette, 1986). The gravity anomalies associated with the individual fracture zone morphology may cause additional lines of the color to be present, but in general, these lines will be subdued and less continuous.

Spreading ridges

As mentioned above, the symbol-switching and the obliqueness with which many of the ridges intersected the satellite tracks made it difficult to identify spreading ridges. As a result, only parts of the Southwest, Central, and Southeast Indian ridges are recognizable on our map. The geoid signature of a ridge, like a fracture zone, depends on the spreading rate. A slow spreading ridge, such as the Southwest Indian Ocean ridge, usually possesses an axial trough which is reflected in the geoid signal (Figure 7). In passing over such a ridge, the satellite first measures an increase in slope, corresponding to a blue lineation on our map, due to the increase in height of the ridge. The maximum downward slope of the axial trough is represented by a red line and the maximum upward slope of the other side of the axial trough is represented by a blue line. As the satellite continues over the other side of the ridge, the maximum downward slope of ridge is represented by a red line. The location of the axial trough is actually between the first red line and the second blue line. This ideal representation is best seen along the Southwest Indian Ridge between the Indomed and Gallieni fracture zones (numbers 24 and 25 in Figure 11).

Seamounts

The seamounts and major island archipelagos are illustrated on the map by small circles and irregular, circular areas (Plate 1). The deflection of the vertical signal for a

Figure 7. The geoid signature of a ridge, like a fracture zone, depends on the spreading rate at the ridge which gives rise to its morphology. A slow spreading ridge, such as shown in this schematic diagram, usually possesses an axial trough which is reflected in the geoid signal. Thus, as the satellite passes over such a ridge, it meausres the positive slope of the ridge (a peak in the deflection of the vertical (DV) signal), the negative slope of the axial trough (a trough in the DV), the positive slope of the trough (a peak in the DV), and the negative slope of the ridge (a trough in the DV). this results in a pattern on the fabric map of blue, red, blue, red. The actual location of the axial trough is at the inflection point in the DV between the negative and positive slopes of the axial trough (i.e., between the first red and second blue line).

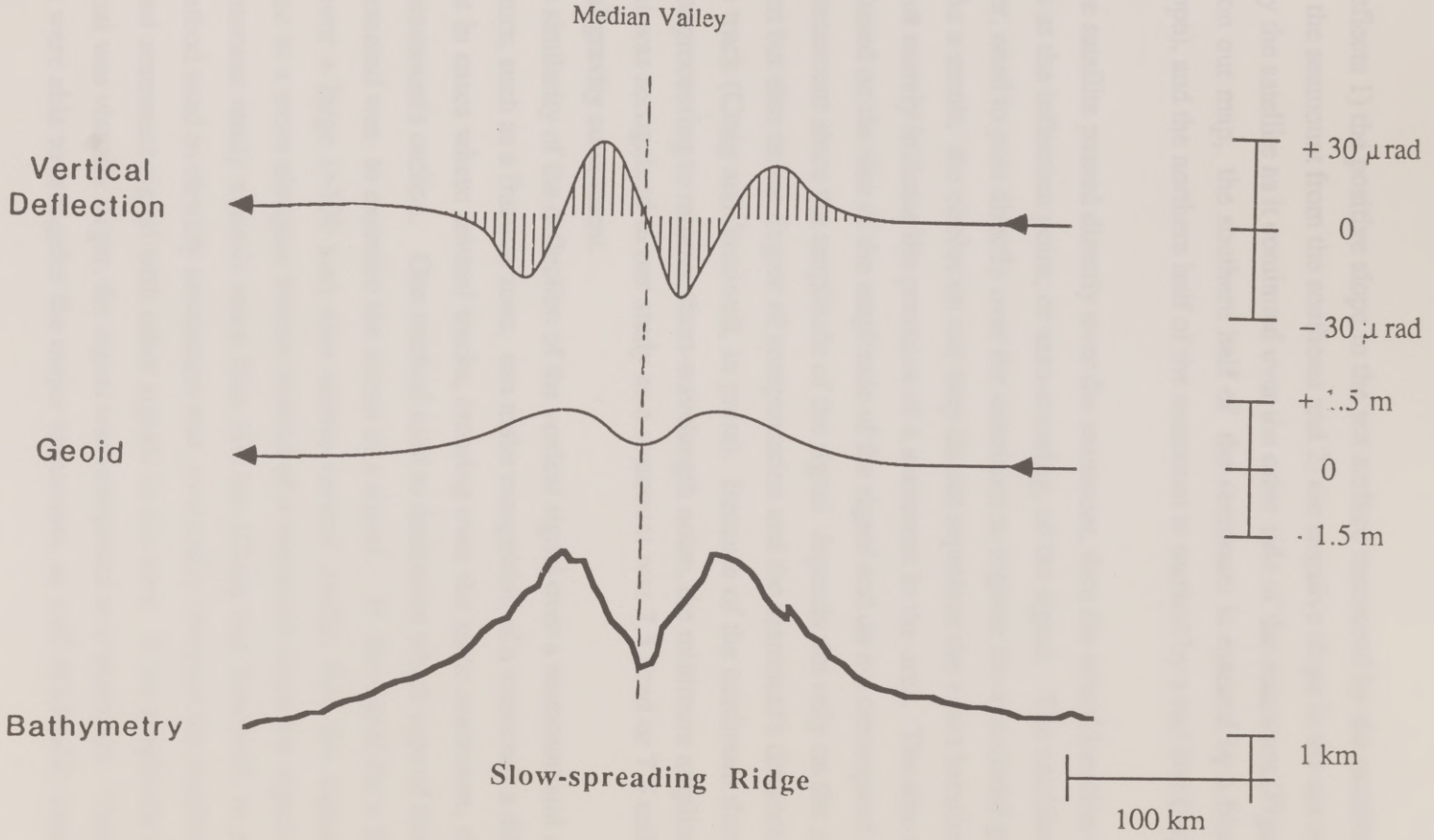
Median Valley
Vertical Deflection
+ 30 μrad
0
– 30 μrad
Geoid
+ 1.5 m
0
- 1.5 m
Bathymetry
1 km
Slow-spreading Ridge
100 km

seamount reflects 1) the positive slope in the sea surface measured by the satellite as it approached the seamount from the southeast and 2) the negative slope in the sea surface measured by the satellite as it continued over the other side of the seamount (Figure 8). Therefore, on our map, the southern half of the seamount is marked by a blue line (positive slope), and the northern half of the seamount is marked by a red line (negative slope).

If the satellite passed directly over the seamount, then the actual location of the seamount is at the inflection point, or zero-crossing, of the signal. The satellite does not, however, need to pass directly over the seamount to register the associated gravity anomaly. As a result, the circles on our map do not represent the exact location of a seamount but merely indicate the presence of a seamount in the area. The size of the circles are based on the size of the amplitude of the signal and do not correspond to the size of the seamount since the amplitude of the signal depends not only on the size of the seamount but also on the degree of compensation and the seamount's distance from the satellite track (Craig and Sandwell, in press). Because of the minimum threshold we set in our processing to remove short-wavelength noise, the minimum amplitude of a signal that was recognized in our study as a seamount was 7.5 μrad or 7.5 milligals of horizontal gravity component.

The similarity of the deflection of the vertical signal over a seamount and across a linear feature, such as a fracture zone, can make recognition of a seamount a difficult task, except in cases where several tracks, crossing over the same seamount, clearly define the seamount's outline. One method used to determine which type of feature a signal represented was to examine the extent of a signal. If the signal for a feature extended over a large (>100 km) area across several tracks, then the signal was probably due to a more elongate feature instead of a seamount since the signal of an isolated seamount rarely extends more than 100 km (Craig and Sandwell, in press). Another method used to identify seamounts was to visually compare the amplitude of the suspected seamount signal with other signals in the area. If the amplitude of the suspect signal was visually larger, the signal was interpreted as a seamount. Using this criteria, we were able to recognize the major seamounts, as well as identify suspected seamounts.

Figure 8. This schematic diagram of a seamount shows how the satellite, in crossing over the seamount, first measures an increase in slope (a peak in the DV and blue on the fabric map) and then measures a decrease in slope (a trough in the DV and red on the map). The seamounts on the fabric map are all represented by circular outlines with blue to the south and red to the north of the seamount.

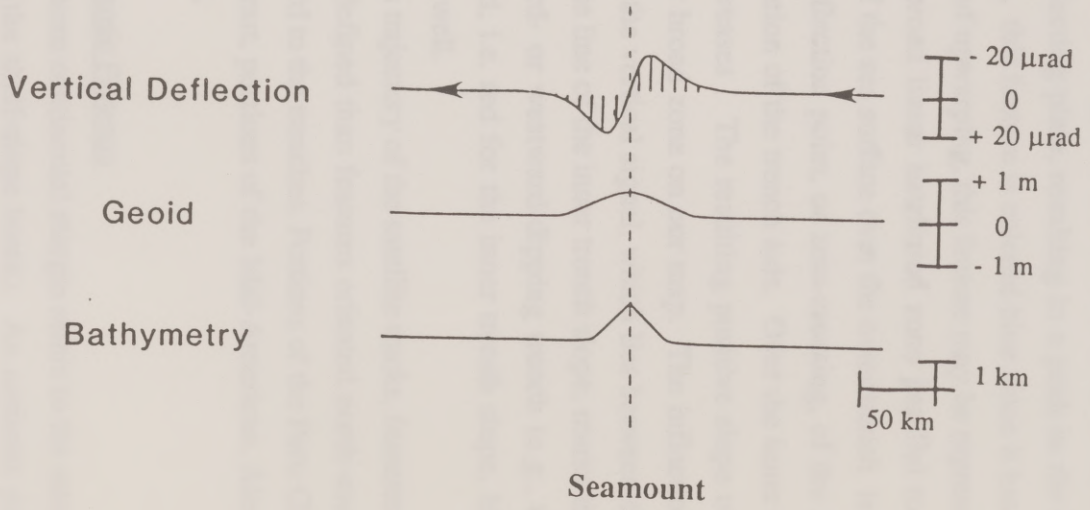
Vertical Deflection
Geoid
Bathymetry
- 20 µrad
0
+ 20 µrad
+ 1 m
0
- 1 m
1 km
50 km
Seamount

Trenches

Our map depicts the deep ocean trenches, which are located near continental margins and island arcs, as linear features. Figure 9 displays a schematic diagram of the generalized bathymetry and associated geoid signal of the area around a northward- or westward-dipping trench. The height of the sea surface increases in response to the slight upwarping of the subducting plate, resulting in a peak in the deflection of the vertical signal. On our map, this feature is colored blue since it has a positive slope. Depending on the magnitude of upwarping, this feature may be represented on our map as either a single line or a broad linear hatchured zone parallel to the trench. The maximum downward slope of the sea surface over the outer trench is represented by a red line on our map. The inflection point, or zero-crossing, of the deflection of the vertical signal marks the location of the trench axis. Over the inner trench slope, the height of the sea surface increases . The resulting positive slope of the sea surface corresponds to a blue line or broad zone on our map. The inflection point, or zero-crossing, of the deflection of the vertical signal, which lies between the red line of the outer trench slope and the blue line of the inner trench slope, marks the location of the trench axis. For a southward- or westward-dipping trench (e.g., the colors of the lineations would be switched, i.e. red for the inner trench slope, blue for the outer trench slope, and red for the swell.

Due to the north-south trajectory of the satellite tracks, features that are oriented east-west are more clearly defined than features oriented north-south. This bias is particularly evident with regard to the trenches. Portions of the Peru-Chile trench trench are not well defined. In contrast, portions of the Mid-American, Aleutian, and Kurile trenches are clearly delineated.

Continental Margins and Aseismic Plateaus

For our purposes, the term continental margin refers to the steepest bathymetric gradient around a continent (the shelf-slope break). An aseismic plateau refers to a submarine feature, other than the mid-ocean ridges, which may be of either continental

Figure 9. A schematic diagram of the bathymetry, geoid signal, and deflection of the vertical signal of a trench.

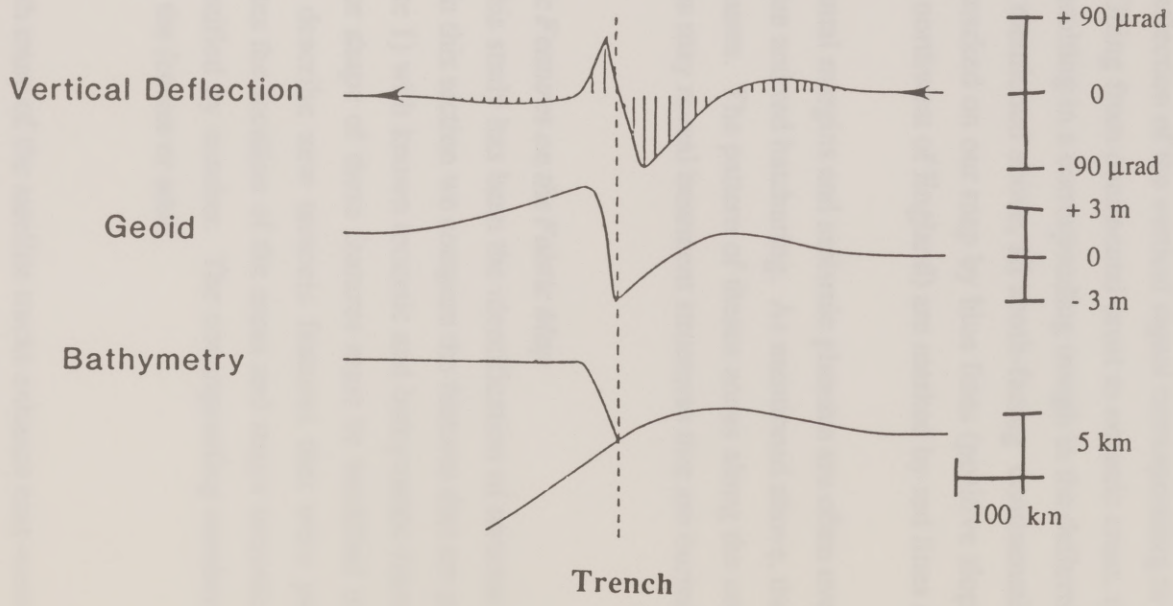
Vertical Deflection
Geoid
Bathymetry
+ 90 µrad
0
- 90 µrad
+ 3 m
0
- 3 m
5 km
100 km
Trench

or oceanic origin. The map presented in this study reveals information on both the outline and the apparent structure along continental margins and on aseismic plateaus.

Figure 10 shows a schematic outline of the bathymetry and geoid signal over a continental margin. As the satellite, travelling northwards, crosses over the continental margin from oceanic crust to continental crust, the height of the sea surface increases. This results in a peak in the deflection of the vertical signal corresponding to the point of maximum positive slope. Going from continental crust to oceanic crust, the height of the sea surface decreases, resulting in a corresponding trough in the deflection of the vertical signal. Therefore, as mentioned above, all south-facing continental margins (e.g., south of Australia) are marked on our map by blue lines (positive slope), while all north-facing margins (e.g., northwest of England) are marked by red lines (negative slope).

The outlines of continental margins and aseismic plateaus are often overprinted, however, by broad zones of blue and red hatchuring. As mentioned above, these zones may be due to a number of causes. The pattern of theses zones along the continental margins suggests that the zones may reveal basement structures that are buried beneath the sedimentary cover.

Identification of Major Tectonic Features on the Fabric Map

The primary goal of this study has been the identification of tectonic features from satellite altimetry data. In this section we compare the features that are present on the Tectonic Fabric Map (Plate 1) with known tectonic and bathymetric features. We also discuss how the extent or shape of these features must be modified in light of satellite altimetry data, and describe new tectonic features that were previously unmapped. Figure 11 illustrates the location of the areas and major tectonic features discussed in this section, identified by number. The corresponding numbers will be displayed in brackets ([]) after the feature or area.

Atlantic Ocean

Because the north-south trend of the satellite tracks enhance east-west trending features, the fracture zones in the Atlantic Region are clearly visible (Plate 1). These include the Charlie Gibbs [102], Kurchatov [103], Pico [104], East Azores [105],

Figure 10. A schematic diagram of the bathymetry, geoid signal, and deflection of the vertical signal across a continental margin (after Heezen, 1962 and Kennett, 1982).

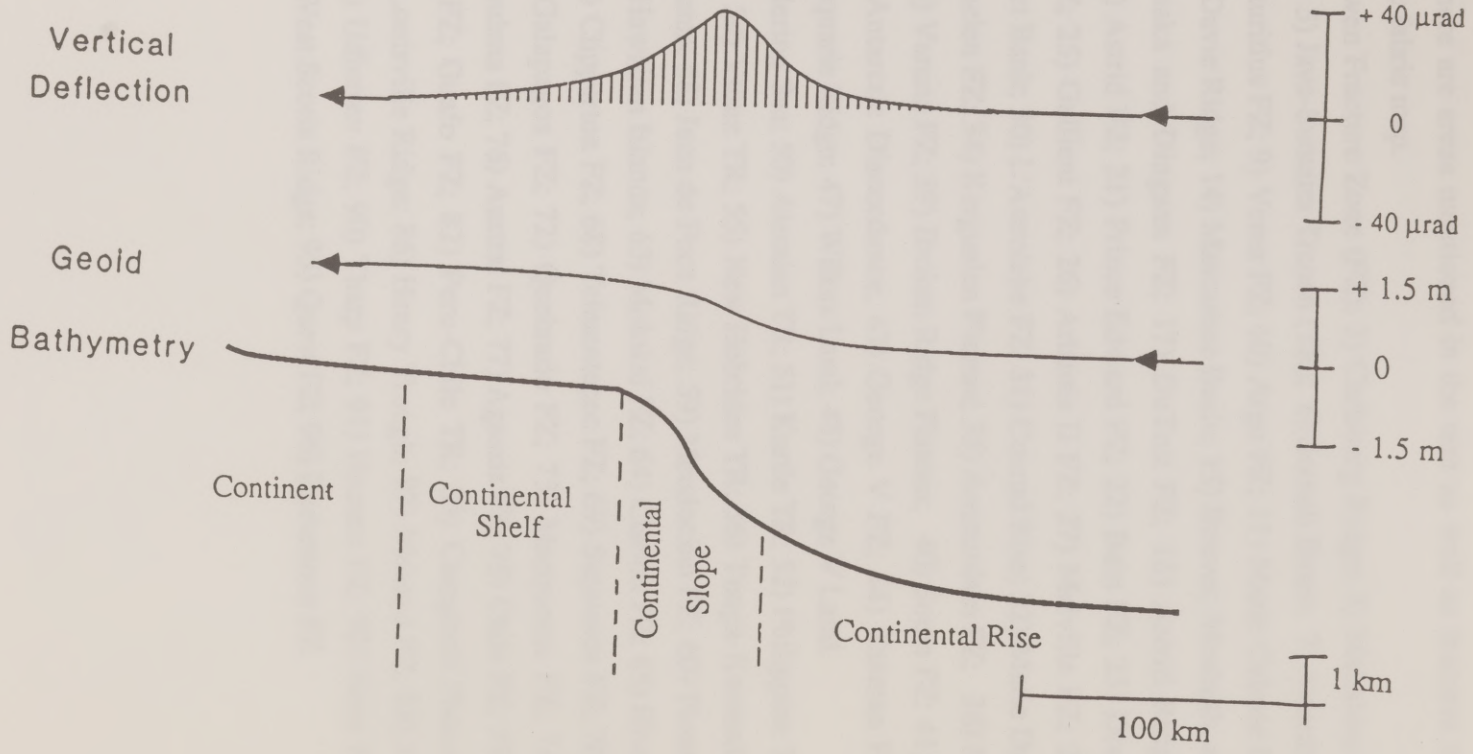
Vertical
Deflection
+ 40 µrad
0
- 40 µrad
Geoid
+ 1.5 m
Bathymetry
0
- 1.5 m
Continent
Continental
Shelf
Continental
Slope
Continental Rise
1 km
100 km

Figure 11. Shown here are areas mentioned in the text as well as features that are visible on the tectonic fabric map.

Indian Ocean: 1) Owen Fracture Zone (FZ); 2) Carlsberg Ridge; 3) Mabahiss FZ; 4) Central Indian Basin; 5) Java-Sumatra Trench (TR); 6) Somali Basin; 7) Amirante TR; 8) Mahanoro and Mauritius FZ; 9) Vema FZ; 10) Argo FZ; 11) Marie Celeste FZ; 12) Investigator FZ; 13) Davie Ridge; 14) Mascarene Basin; 15) Bouvet, Moshesh, and Isla Orcadas FZ; 16) Shaka and Dingaan FZ; 17) DuToit FZ; 18) Astrid Ridge; 19) Gunnerus Ridge; 20) Astrid FZ; 21) Prince Edward FZ; 22) Bain FZ; 23) Discovery FZ; 24) Indomed FZ; 25) Gallieni FZ; 26) Atlantis II FZ; 27) Melville FZ; 28) Del Caño Rise; 29) Crozet Bank; 30) L'Astrolabe FZ; 31) Conrad Rise; 32) Marie Dufresne Seamount; 33) Kerguelen FZ; 34) Kerguelen Plateau; 35) Amsterdam FZ; 36) St. Paul FZ; 37) Mitra FZ; 38) Varuna FZ; 39) Broken Ridge Plateau; 40) Soma FZ; 41) Surya FZ; 42) Australian-Antarctic Discordance; 43) George V FZ; 44) Tasman FZ; 45) Balleny FZ; 46) Macquarie Ridge; 47) Wilkes Land; 48) George V Land.

Pacific Ocean: 49) Bering Sea; 50) Aleutian TR; 51) Kurile TR; 52) Philippine TR; 53) South Solomon TR; 54) Vitiaz TR; 55) New Hebrides TR; 56) Tonga-Kermadec TR; 57) Emperor Seamounts; 58) Juan de Fuca Ridge; 59) Mendocino FZ; 60) Pioneer FZ; 61) Murray FZ; 62) Hawaiian Islands; 63) Molokai FZ; 64) Clarion FZ; 65) Rivera FZ; 66) Line Islands; 67) Clipperton FZ; 68) Tehuantepec FZ; 69) Siquieros FZ; 70) Mid-American TR; 71) Galapagos FZ; 72) Quebrado FZ; 73) Marquesas FZ; 74) East Pacific Rise; 75) Mendana FZ; 76) Austral FZ; 77) Agassiz FZ; 78) Chile FZ; 79) Chile Rise; 80) Valdivia FZ; Guafo FZ; 82) Peru-Chile TR; 83) Campbell Plateau; 84) Chatham Rise; 85) Louisville Ridge; 86) Henry Trough; 87) Menard FZ; 88) Pacific-Antarctic Ridge; 89) Udintsev FZ; 90) Tharp FZ; 91) Heezen FZ; 92) Hero FZ; 93) Shackleton FZ; 94) West Scotia Ridge; 95) Quest FZ; 96) Endurance FZ.

Atlantic Ocean: 97) Baffin Bay; 98) Reykjanes Ridge; 99) Faeros Ridge; 100) Labrador Sea; 101) Bight FZ; 102) Charlie Gibbs FZ; 103) Kurchatov FZ; 104) Pico FZ; 105) East Azores FZ; 106) Oceanographer FZ; 107) Hayes FZ; 108) Cruiser FZ; 109) Atlantis FZ; 110) Tyro FZ; 111) Kane FZ; 112) Gulf of Mexico; 113) Cayman Trough; 114) Hess Escarpment; 115) Muertos Trough; 116) Puerto Rico TR; 117) Atlantic Ridge; 118) Jacksonville FZ; 119) Fifteen-Twenty FZ; 120) Vema FZ; 121) Sierra Leone FZ; 122) Four North FZ; 123) St. Paul FZ; 124) Romanche FZ; 125) Ascension FZ; 126) Bode Verde FZ; 127) St. Helene; 128) Hotspur FZ; 129) Martin Vaz FZ; 130) Rio de Janeiro FZ; 131) Rio Grande Ridge; 132) Rio Grande FZ; 133) Salado Basin; 134) Colorado Basin; 135) Tristan da Cunha FZ; 136) Falkland -Agulhas FZ; 137) South Sandwich TR; 138) Conrad FZ; 139) Bullard FZ; 140) South Sandwich FZ; 141) Weddell Sea; 142) Walvis Ridge.

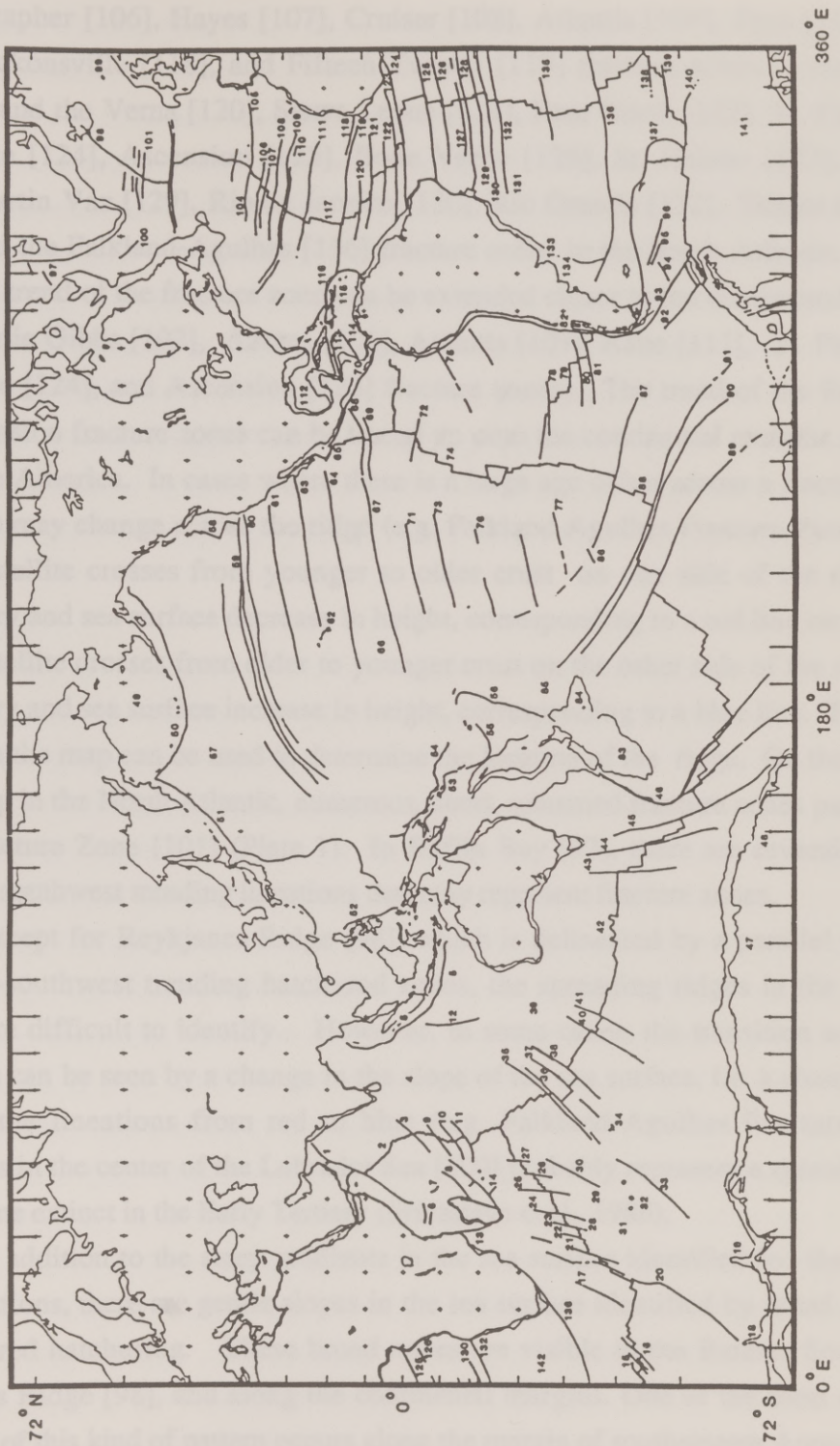
72°N
0°
72°S
0°E
180°E
360°E

Oceanographer [106], Hayes [107], Cruiser [108], Atlantis [109], Tyro [110], Kane [111], Jackonsville [118], and Fifteen-Twenty [119] fracture zones in the Central Atlantic, and the Vema [120], Sierra Leone [121], Four North [122], St. Paul [123], Romanche [124], Ascension [125], Bode Verde [126], St. Helene [127], Hotspur [128], Martin Vaz [129], Rio de Janeiro [130], Rio Grande [132], Tristan da Cunha [135], and the Falkland-Agulhas [136] fracture zones in the South Atlantic. In many cases, the trend of the fracture zone can be extended closer to the continental margins (e.g. Charlie Gibbs [102], Azores [105], Atlantis [109], Kane [111], St. Paul [123], Romanche [124], and Ascension [125] fracture zones). The trend of the Romanche and Ascension fracture zones can be traced up onto the continental margins of Africa and South America. In cases where there is a large age offset across a fracture zone, the colors may change across the ridge (e.g. Falkland-Agulhas Fracture Zone [136]). As the satellite crosses from younger to older crust on one side of the ridge, the bathymetry and sea surface decrease in height, corresponding to a red line on the map. As the satellite crosses from older to younger crust on the other side of the ridge, the bathymetry and sea surface increase in height, corresponding to a blue line. This color change on the map can be used to determine the location of the ridge. On the tectonic fabric map in the North Atlantic, numerous, short, unnamed fracture zones parallel the Bight Fracture Zone [101] (Plate 1). In Baffin Bay [97], there are several pairs of northeast-southwest trending lineations that may represent fracture zones.

Except for Reykjanes Ridge [98], which is delineated by a parallel series of northeast-southwest trending hatchured zones, the spreading ridges in the Atlantic Region are difficult to identify. However, in some cases, the transition across the ridge axis can be seen by a change in the slope of the sea surface, i.e. a change in the color of the lineations from red to blue (e.g. Falkland-Agulhas Fracture Zone). Lineations in the center of the Labrador Sea [100] probably represent a spreading axis that became extinct in the Early Tertiary (Srivastava et al., 1986).

In addition to the steep gradients in the sea surface identified by the red and blue lineations, there are gentle slopes in the sea surface identified by broad zones of blue and red hatchuring. These broad zones are visible in the Barents Sea, on the Reykjanes Ridge [98], and along the continental margins. One of the most dramatic examples of this kind of pattern occurs along the margin of southeastern Argentina and

the Falkland Plateau (Plate 1). In this area the red and blue hatchuring probably represents basement structures that are buried beneath a thin veneer of sediments (e. g. Salado [133] and Colorado [134] basins). These zones of red and blue hatchuring also extend into the ocean basins, where they usually correspond to volcanic edifices and aseismic plateaus (Rio Grande [131] - Walvis Ridge [142], Faeroes Ridge [99]).

The complex pattern of the tectonic fabric in the Caribbean and Gulf of Mexico [112] region is due to a variety of tectonic features. The lineations that are parallel to the margins of the Gulf of Mexico represent stretched continental crust, as well as a narrow zone of oceanic crust that lies in the center of the Gulf (Buffler and Sawyer, 1983). The Cayman Trough [113] and Hess Escarpment [114] are well-defined by sets of parallel lineations. The Muertos Trough [115], south of Hispaniola, and the Puerto Rico Trench [116] are outlined by broad swells in the slope of the sea surface (Plate 1).

Indian Ocean

Unlike the tectonic fabric of the Atlantic, which is dominated by fracture zone trends, the tectonic fabric of the Indian Ocean reveals a variety of tectonic features. These features include: young and old fracture zones, active and extinct spreading centers, volcanic features, aseismic plateaus, rifted continental margins and trenches.

The fracture zone lineations in the Indian Ocean are generally more difficult to identify due to their primarily north-south orientation. However, distinct fracture zone trends can be recognized in the vicinity of slow spreading ridges. Along the Central Indian Ridge, the Owen [1], Mabahiss [3], Vema [9], Argo [10], and Marie Celeste [11] fracture zones can be identified. Along the Southwest Indian Ridge, the Melville [27], Atlantis II [26], Gallieni [25], Indomed [24], Discovery [23], Prince Edward [21], Bain [22], and DuToit [17] fracture zones are recognizable. The L'Astrolabe Fracture Zone [30] to the south of the Southwest Indian Ridge is also visible. Although located in a faster spreading regime, several fracture zones along the Southeast Indian Ridge can be identified: the Amsterdam 35], St. Paul [36], Mitra [37], Varuna [38], Soma [40] and Surya [41] fracture zones (McKenzie and Sclater, 1971). Using satellite altimetry data, the trends of several fracture zones can be extended closer to the continental margins (e.g. George V [43], Tasman [44], and Balleny [45] fracture zones). Older fracture zones, such as the Davie Ridge [13] in the

Somali Basin [6], and the Mauritius and Mahanoro fracture zones [8] south of the Mascarene Basin [14] are visible on the tectonic fabric map (Plate 1). The bends in the red and blue lineations corresponding to the Astrid [18] and Investigator [12] fracture zones reveal major changes in spreading direction.

Portions of the Central, Southwest and Southeast Indian ridges, due to their east-west orientation, can be identified on the tectonic fabric map. The most easily identified ridge segments are located along the southeast portion of the Carlsberg Ridge [2], along the Southeast Indian Ridge south of the Agulhas Basin, between the Indomed Fracture Zone [24] and Central Indian Triple Junction, and along the Australian-Antarctic Discordance [42]. South of Réunion Island, the extinct spreading center in the Mascarene Basin [14] (Schlich, 1982) is outlined by two pairs of northwest-southeast trending red and blue lineations.

As in the Atlantic region, the blue and red hatchured zones represent broad, gently sloping areas of the sea surface. In the Indian Ocean, the most prominent of these features correspond to the Kerguelen [34] and Broken Ridge [39] plateaus (Plate 1). Using the satellite altimetry data, the extent of the Kerguelen Plateau has been mapped in detail, and a variety of associated features, such as the Labuan Basin and Elan Bank, have been identified (Coffin et al., 1986). Other features, such as the Del Caño Rise [28], Crozet Bank [29] and the Conrad Rise [31], are clearly visible on the fabric map, and new seamounts have been identified northeast of Marion Dufresne Seamount [32]. Though the Ninetyeast Ridge and Chagos-Laccadive Ridge are major tectonic features, they do not appear on our tectonic fabric map because of their orientation.

The continental margins of Antarctica (Wilkes Land [47]) and southern Australia display hatchured zones that may correspond to broad areas of stretched continental or transitional crust or marginal sedimentary basins. Similar hatchured areas along the eastern margin of India and south of Pakistan may be related to the progradation of the Ganges and Indus fans. Of particular interest is the set of east-west trending hatchured zones in the Central Indian Basin [4]. These features represent the buckling and folding of oceanic crust related to the ongoing collision of India and Eurasia (Weissel et al., 1980; McAdoo and Sandwell, 1985).

The Java - Sumatra [5] trenches are illustrated on the tectonic fabric map by a series of arcuate lineations. Similar lineations are observed along the Seychelle Islands south of the Amirante Trench [7].

Pacific Ocean

The tectonic fabric of the western and central Pacific is dominated by irregular or circular features representing seamounts. Several subparallel seamount trends can be recognized. The most prominent seamount trends are associated with the Hawaiian [62]-Emperor [57] archipelago, the Line Islands [66], the Austral Islands, Easter Island, and the Louisville Ridge [85] (Craig and Sandwell, in press).

In contrast, the most prominent tectonic fabric in the eastern Pacific basin are the satellite altimetry lineations associated with fracture zones. In the Northeast Pacific, tectonic lineations associated with the Mendocino [59], Pioneer [60], Murray [61], Molokai [63], Clarion [64], Rivera [65], Clipperton [67], Tehuantepec [68], and Siquieros [69] fracture zones are clearly visible. Our interpretation of the satellite altimetry data suggests that the Mendocino Fracture Zone [59] can be extended west of the Emperor Islands [57], the Murray [61] and Molokai [63] fracture zones can be extended to the Hawaiian Islands [62], and the Clipperton Fracture Zone [67] may extend west of the Line Islands [66] (Plate 1). In the Southeast and Southwest Pacific, the Galapagos [71], Marquesas [73], Quebrada [72], Mendana [75], Chile [78], Valdivia [80], Guafo [80], Austral [76], Agassiz [77], Menard [87], Heezen [91], Tharp [90], Udintsev [89], and Hero [92] fracture zones can be identified on the tectonic fabric map (Plate 1). The Marquesas [73], Austral [76], and Guafo [80] fracture zones, in particular, can be mapped in greater detail than is available from bathymetric maps. In the Southwest Pacific, numerous fracture zone lineations have been identified that lie parallel to the major fracture zones (Heezen [91], Tharp [90], and Udintsev [89] fracture zones). In most cases, the trends of these fracture zones can be extended nearly to the margin of Antarctica.

Due to its low relief and predominantly north-south orientation, the East Pacific Rise [74] is not visible on the tectonic fabric map. Similarly, the Juan de Fuca Ridge [58], Chile Rise [79] and the Pacific-Antarctic Ridge [88] can not be mapped directly. The locations of these spreading centers, however, often can be inferred by noting the

change in the slope of the sea surface along fracture zones near the ridge axis. The ridge can be located by observing where the lineation changes from red to blue (e.g. along Udintsev Fracture Zone[89] at 55° S, 145°W).

Another rift-related feature, the Henry Trough [86] (45° S, 135° W), is clearly visible on the tectonic fabric map (Plate 1). The L-shape bend south of the Menard Fracture Zone [87] marks the location where a propagating ridge rifted older oceanic crust (Cande et al., 1982). The satellite-derived lineations are well-defined in this region due to the contrasting ages of the oceanic crust (60 Ma vs. 47 Ma).

As expected, the trenches are best expressed where the satellite tracks cross the trench at a high angle (Aleutian [50], Kurile [51], South Solomon [53], Vitiaz [54], New Hebrides [55], and Mid-American [70] trenches). The expression of the trench is more subdued where the satellite tracks run subparallel to the trench axis (Philippine [52], Tonga-Kermadec [56], Peru-Chile [82] trenches). The trench axis is marked by a single, red line. Along some trenches (Aleutian [50], Kurile [51], and New Hebrides [55]), a broad positive anomaly in the slope of the sea surface is present seaward of the trench (blue hatchuring). This anomaly is probably due to the bending and upwarping of the subducting oceanic lithosphere.

Other broad areas of hatchuring, indicating gentle slopes of the sea surface, are present in the Pacific. The hatchuring over the Campbell Plateau [83] and Chatham Rise [84] (New Zealand) is similar to the tectonic fabric over the Falkland Plateau , and probably represents basement structures associated with stretched continental or transitional crust. Similar features are observed in the Bering basin [49] and along the Bering shelf margin.

Circum-Antarctic Region

As discussed in the introduction, because the Seasat mission was in operation during the Austral winter, the results from high southerly latitudes (>60°S) were degraded by the effects of sea ice. The Geosat mission, however, collected data during the Austral summer; as a result, the information from high southerly latitudes is exceptionally good. Numerous new tectonic features can be identified using the Geosat data (Sandwell and McAdoo, in press). These features provide important constraints for the development of the Antarctic margin, and the evolution of the southern oceans.

In the South Atlantic, the distinct fracture zone pattern surrounding the Bouvet triple junction is clearly visible (Plate 1). Of particular interest is the fracture zone pattern associated with the American-Antarctic Ridge (Barker and Lawver, in press). The northwest-southeast trend of this fabric extends southward into the Weddell Sea [141], and ultimately to the continental margin of Antarctica.

East of the Weddell Sea, the tectonic fabric changes abruptly. A new set of northeast-southwest trending fracture zones intersects the Weddell Sea fracture zone lineaments. The most continuous lineament, the Astrid Fracture Zone [20], can be traced northward from the Astrid Ridge [18], across the Southwest Indian Ridge and towards the Mozambique Escarpment. This lineament is a flow-line that records the relative movement of Africa with respect to Antarctica since the Late Jurassic (Bergh, 1987).

Another lineament is observed east of the Gunnerus Ridge [19], to the southwest of the Kerguelen Plateau [34]. This lineament, the Kerguelen Fracture Zone [33], is the flow-line that records the relative movement of India with respect to Antarctica since the Early Cretaceous (Royer et al., in prep). It forms the western boundary of the Kerguelen Plateau [34]. The conjugate portion of the Kerguelen Fracture Zone [33] on the Indian plate is difficult to identify, however, the matching fracture zone probably lies to the west of the Ninety-East Ridge.

A third set of lineaments have been mapped between Australia and Antarctica. The most prominent fracture zone lineations in this set (George V [43], Tasman [44], and Balleny [45] fracture zones) run from southeast Australia to George V Land [48], Antarctica. These fracture zone lineations are flow-lines that record the relative movement of Australia and Antarctica since the Late Cretaceous (Weissel and Hayes, 1972; Cande and Mutter,1982). The broad zones of blue and red hatchuring along the coast of George V Land [48] and the south coast of Australia probably represent stretched continental or transitional crust formed during the earliest phases of rifting.

East of the Balleny Fracture Zone [45], the Macquarie Ridge [46] can be easily identified by a set of arcuate lineations. Further to the east, in the southwest Pacific Basin, a dense northwest-southeast trending fracture zone fabric has been mapped. These fracture zone trends are parallel to the Udintsev [89], Tharp [90] and Heezen [91] fracture zones, and extend the known limit of these fracture zones to higher

latitudes. The southward extension of the Udintsev Fracture Zone [90] intersects the margin of western Antarctica at Pine Island Bay, between Thurston Island and Marie Byrdland (Sandwell and McAdoo, in press).

In the Scotia Sea, the Shackleton [93], Quest [95] and Endurance [96] fracture zones have been identified. Though the present-day spreading center is not recognized, the West Scotia Ridge [94], an extinct, northeast-southwest trending ridge can be seen on the fabric map (Plate 1) (Barker and Burrell, 1977).

Summary and Conclusions

Although most of the tectonic features cited above have been previously known or suspected from ship-track data, the satellite altimetry data enhances our knowledge of them. The tectonic fabric map provides a greater resolution of the outline of many of these features while also permitting the extension of the physical limits of certain features beyond what bathymetric charts show. This new information will no doubt play a part in various aspects of plate tectonic modelling, in particular, the detail and extension of fracture zone lineations, which have recorded plate movement through time, may serve as additional constraints for plate reconstruction.

Besides providing more detail on known features, the tectonic fabric map also displays features that are not apparent on global bathymetric maps (GEBCO). The satellite data reveal the presence of numerous seamounts in the north and central Pacific and the distinct lack of seamounts in the southern oceans (Craig and Sandwell, in press). As mentioned above, the extinct spreading center in the Mascarene Basin and portions of the Southeast Indian ridge at the Australian-Antarctic Discordance are visible on the map.

Due to the lack of ship-track data in the southern oceans, the satellite data reveal several pieces of information on fracture zone lineations and trends which are not seen on bathymetric charts. For instance, in between the major fracture zone lineations in the southwest Pacific Ocean are many smaller lineations that may correspond to minor uncharted fracture zones. In the Weddell Sea, the trend of the lineations on the tectonic fabric map reveal the spreading history of the area.

The tectonic fabric map also displays features that are the result of the expression of deep-seated gravity anomalies. These broad geoid anomalies partially define several aseismic plateaus such as the Kerguelen, Broken Ridge, and Campbell plateaus. The anomalies are visible over the continental crust of the Falkland Plateau as well as over the oceanic crust slightly to the north of the plateau. In the Central Indian Ocean, these gravity anomalies appear as wrinkles on the tectonic fabric map (Weissel et al., 1980; Haxby, 1985,1987; McAdoo and Sandwell, 1985).

From our analysis of Seasat and Geosat satellite altimetry data we have been able to map the tectonic fabric of the ocean basins and continental margins. Using the slope of the sea surface (deflection of the vertical) we have identified: fracture zones,

spreading ridges, subducting trenches, seamounts, aseismic plateaus, and deeply buried features along the continental margins. The global uniformity of the spacing of the satellite data allows us to map known features in greater detail and in a more continuous manner, particularly in the southern oceans. The data has given us proof of the continuity of tectonic features that were previously evidenced by irregularly spaced ship-track data or magnetic anomaly offsets, as in the case of the southwestern extent of the L'Astrolabe Fracture Zone. In addition to being able to identify known tectonic features, we have also identified numerous, new tectonic elements. However, we have just barely scratched the surface, and there is no doubt that in the future a wealth of additional information will be revealed by detailed studies of satellite altimetry data. The tectonic fabric map that we present in this paper is a starting point. The tectonic features that we have mapped will be used to: 1) produce more accurate plate tectonic reconstructions, 2) identify epochs of global plate reorganization, and 3) understand the subtle dynamics of the plate tectonic process.

The accuracy of plate tectonic reconstructions depends on the amount of data that "constrains" the fit. The tectonic fabric we have mapped provides numerous additional control points and constraints for high resolution plate tectonic reconstructions. We believe that the fabric itself, has a story to tell. The tectonic fabric records the subtle changes in spreading direction through time. The "bumps and undulations" in the fabric flowlines reflect changes in plate motion. In future studies we hope to correlate "bumps and undulations" between ocean basins, in order to determine if these changes in plate motion were globally synchronous. Finally, as more satellite altimetry data become available, we hope to produce higher resolution tectonic fabric maps. These maps will be an essential tool for understanding the pattern of plate tectonic processes in time and space. Questions such as "How often do ridge jumps occur?"; "How do ridge segments change through time?"; "Do oceanic fracture zones extend onto the continental margins?" and "Are plate tectonic processes continuous or episodic?" may be answered by these global tectonic fabric maps.

Acknowledgements

This work was supported by funding from Amoco International Oil Co., Chevron Overseas Petroleum Co., Conoco, Elf Aquitaine, Exxon Production Research, Mobil Oil Co., PetroCanada, Phillips Petroleum, Shell Development Co., and Standard Oil Co., as part of their sponsorship of the Paleoceanographic Mapping Project, University of Texas at Austin. This work was also partially supported by the NASA Geodynamics Program (NAG5-787). Maps at a scale of 1:10,000,000 of the both the satellite altimetry picks and the interpreted tectonic fabric are available from the authors.

REFERENCES

Barker, P.F. and Burrell, J., 1977. The opening of Drake Passage. Marine Geology, 25: 15-34.

Born, G.H., Mitchell, J.L. and Heyler, G.A., 1987. Design of the Geosat Exact Repeat Mission. John Hopkins APL Technical Digest, 8: 260-266.

Brammer, R.F. and Sailor, R.V., 1980. Preliminary estimates of the resolution capability of the Seasat radar altimeter. Geophys. Res. Lett., 7: 193-196.

Buffler, R.T. and Sawyer, D.S., 1983. Distribution of crust and early history, Gulf of Mexico basin. Gulf Coast Assoc. Geol. Soc. Trans., 35: 334-344.

Cande, S.C., Herron, E.M. and Hall, B.R., 1982. The early Cenozoic tectonic history of the southeast Pacific. Earth Planet. Sci. Lett., 57: 63-74.

Cande, S.C. and Mutter, J.C., 1982. A revised identification of the oldest sea-floor spreading anomalies between Australia and Antarctica. Earth Planet. Sci. Lett., 58: 151-160.

Cande, S.C., LaBrecque, J.L. and Haxby, W.B., in press. Plate kinematics of the South Atlantic: chron 34 to present. J. Geophys. Res.

Coffin, M.F., Davies, H.L. and Haxby, W.F., 1986. Structure of the Kerguelen plateau province from Seasat altimetry and seismic reflection data. Nature, 324: 134-136.

Collette, B.J., 1986. Fracture zones in the North Atlantic: morphology and a model. J. Geol. Soc. London, 143: 763-774.

Craig, C.H. and Sandwell, D.T., in press. The global distribution of seamounts from Seasat profiles. J. Geophys. Res.

Gahagan, L.M., 1988. Tectonic features in the ocean basins from satellite altimetry data. Master's thesis, The University of Texas at Austin.

Haxby, W.F., Karner, G.D., LaBrecque, J.L. and Weissel, J.K., 1983. Digital images of combined oceanic and continental data sets and their use in tectonic studies. EOS, 64: 995-1004.

Haxby, W.F., 1985. Gravity Field of the World's Oceans. Lamont-Doherty Geol. Obs., Palisades, New York.

Haxby, W.F., 1987. Gravity field of the world's oceans. NOAA Report MGG-3.

Hancock, D.W., Forsythe, R.G. and Lorell, J., 1980. Seasat altimeter sensor file algorithms. IEEE Oceanic Eng., OE 5(2), pp. 93-99.

Heezen, B.C., 1962. The Deep Sea Floor, in S.K. Runcorn (Editor), Continental Drift, pp. 235-288, Academic Press, New York.

Jensen, J.J. and Wooldridge, F.R., 1987. The Navy Geosat mission: an introduction. John Hopkins APL Technical Digest, 8: 169.

Kennett, J.P., 1982. Marine Geology, p. 27, Prentice-Hall, Inc., New Jersey.

Lame, D.B. and Born, G.H., 1982. Seasat measurement system evaluation: achievements and limitations. J. Geophys. Res., 87: 3175-3178.

Lawver, L.A., Royer, J.Y., Sandwell, D.T. and Scotese, C.R., in press. Evolution of the Antarctic continental margins. Fifth International Antarctic Earth Sciences Symposium, Cambridge, UK.

Lorell, J., 1980. Algorithm development facility altimeter sensor algorithm specifications. JPL Intern. Rep. 622-2071, revision a, Jet Propul. Lab., Pasadena, Calif.

MacArthur, J.L., Marth, Jr., P.C. and Wall, J.G., 1987. The Geosat Radar Altimeter. John Hopkins APL Technical Digest, 8: 176-181.

Marks, K.M. and Sailor, R.V., 1986. Comparison of GEOS-3 and Seasat altimeter resolution capabilities. Geophys. Res. Lett., 13: 697-700.

McAdoo, D.C., 1981. Geoid anomalies in the vicinity of subduction zones. J. Geophys. Res., 86: 6073-6090.

McAdoo, D.C. and Sandwell, D.T., 1985. Folding of Oceanic Lithosphere. J. Geophys. Res., 90: 8563-8569.

McConathy, D.R. and Kilgus, C.C., 1987. The Navy Geosat mission: an overview. John Hopkins APL Technical Digest, 8: 170-175.

McKenzie, D. and Sclater, J.G., 1971. The evolution of the Indian Ocean since the Late Cretaceous. Geophys. J. Roy. Astr. Soc., 25: 437-528.

Mitchell, J.L., Hallock, Z.R. and Thompson, J.D., 1987. REX and Geosat: progress in the first year. John Hopkins APL Technical Digest, 8: 234-244.

Parke, M.E., Born, G.H. and Scott, J.F., 1980. Seasat altimeter geophysical algorithm specifications. JPL Intern Rep. 622-226, Jet Propul. Lab., Pasadena, Calif.

Royer, J.Y. and Sandwell, D.T., in prep. Evolution of the Eastern Indian Ocean Since the Late Cretaceous: Constraints from Geosat altimetry.

Sailor, R.V. and LeSchack, A.R., 1987. Preliminary Determination of the Geosat radar altimeter noise spectrum. John Hopkins APL Technical Digest, 8: 182-183.

Sailor, R.V. and Okal, E.A., 1983. Applications of Seasat altimeter data in seismotectonic studies of the South-Central Pacific. J. Geophys. Res., 88: 1572-1580.

Sandwell, D.T., 1984a. A detailed view of the South Pacific geoid from satellite altimetry. J. Geophys. Res., 89: 1089-1104.

Sandwell, D.T., 1984b. Along-track deflection of the vertical from Seasat: GEBCO overlays. NOAA Technical Memorandum NOS NGS-40.

Sandwell, D.T. and McAdoo, D.C., in press. Marine gravity of the Southern Ocean and Antarctic margin from Geosat. J. Geophys. Res.

Srivastava, S.P. and Tapscott, C.R., 1986. Plate kinematics of the North Atlantic. In P.R. Vogt and B.E. Tucholke (Editors), The western North Atlantic region. GSA DNAG Series Vol. M, 379-404.

Tapley, B.D., Born, G.H. and Parke, M.E., 1982. The Seasat altimeter data and its accuracy assessment. J. Geophys. Res., 87: 3179-3188.

Van Hee, D.H., 1987. Preliminary results from the processing of a limited set of Geosat radar altimeter data. John Hopkins APL Technical Digest, 8: 201-205.

Weissel, J.K., Anderson, R.N. and Geller, C.A., 1980. Deformation of the Indo-Australian plate. Nature, 287: 284-291.

Weissel, J.K. and Hayes, D.E., 1972. Magnetic anomalies in the southeast Indian Ocean. In D.E. Hayes (Editor), Antarctic Oceanology II: the Australian - New Zealand Sector. Antarct. Res. Ser., 19: 165-196.

V. References

Berggren, W.A., Kent, D.V., Flynn, J.J., and van Couvering, J.A., 1985. Cenozoic geochronology, GSA Bull., 96(11), 1407-1418.

Brammer, R.F. and Sailor, R.V., 1980. Preliminary estimates of the resolution capability of the Seasat radar altimeter. Geophys. Res. Lett., 7: 193-196.

Cande, S.C., LaBrecque, J.L. and Haxby, W.B., in press. Plate kinematics of the South Atlantic: chron 34 to present. J. Geophys. Res.

Craig, C.H. and Sandwell, D.T., in press. The global distribution of seamounts from Seasat profiles. J. Geophys. Res.

Dixon, T.H. and Parke, M.E., 1983. Bathymetry estimates in the southern oceans from Seasat altimetry, Nature, 304: 407-409.

Driscoll , M.L., Fisher, R.L., and Parsons, B., in press. Fracture zone trends and structure at the Southwest Indian Ridge: An investigation using Seasat altimetry and surface-ship bathymetry. Geophys. J. Royal Astr. Soc.

Fisher, R.L. and Sclater, J.G., 1983. Tectonic evolution of the Southwest Indian Ocean since the Mid-Cretaceous: Plate motions and stability of the pole of Antarctica/Africa for at least 80 Myr, Geophys. J. R. Astr. Soc., 73: 553-576.

Gahagan, L.M., Royer, J.-Y., Scotese, C.R., Sandwell, D.T., Winn, J.K., Tomlins, R.L., Ross, M.I., Newman, J.S., Müller, R.D., Mayes, C.L., Lawver, L.A., and Heubeck, C.E., in press. Tectonic fabric map of the ocean basins from satellite altimetry data, Tectonophysics.

General Bathymetric Chart of the Oceans (5th Edition), 1984. International Hydrographic Organization / Intergovernmental Oceanic Commission / Canadian Hydrographic Service, Ottawa, Canada. Scale 1:35,000,000 and 1:10,000,000.

Haxby, W.F., Karner, G.D., LaBrecque, J.L., and Weissel, J.K., 1983. Digital images of combined oceanic and continental data sets and their use in tectonic studies, EOS Trans. Am. Geophys. Union, 64: 995-1004.

Haxby, W.F., 1985. Gravity Field of the World's Oceans. Lamont-Doherty Geol. Obs., Palisades, New York.

Haxby, W.F., 1987. Gravity field of the world's oceans. NOAA Report MGG-3.

Hilde, T.W.C., Isezki, N., and Wageman, J.M., 1976. AGU Geophys. Mono. 19, in The Geophysics of the Pacific Ocean Basin and its Margins, pp. 205-226.

Jensen, J.J. and Wooldridge, F.R., 1987. The Navy Geosat mission: an introduction. John Hopkins APL Technical Digest, 8: 169.

Lame, D.B. and Born, G.H., 1982. Seasat measurement system evaluation: achievements and limitations. J. Geophys. Res., 87: 3175-3178.

Larson, R.L., Pitman, W.C., III, Golovchenko, X., Cande, S.C., Dewey, J.F., Haxby, W.F. and LaBrecque, J.L., 1985. The Bedrock Geology of the World. Freeman, New York.

MacArthur, J.L., Marth, Jr., P.C. and Wall, J.G., 1987. The Geosat Radar Altimeter. John Hopkins APL Technical Digest, 8: 176-181.

Mammerickx, J., Smith, S.M., Taylor, I.L., and Chase, T.E., 1974. Bathymetry of the South Pacific, report, La Jolla Inst. Mar. Resour., Univ. Calif., San Diego.

Mammerickx, J., Taylor, I.L., and Cande, S., 1984. GEBCO Panel 5•15, IHO/IOC/CHS, GEBCO - General Bathymetric Chart of the Oceans (5th Edition), International Hydrographic Organization / Intergovernmental Oceanic Commission / Canadian Hydrographic Service, Ottawa, Canada.

Marks, K.M. and Sailor, R.V., 1986. Comparison of GEOS-3 and Seasat altimeter resolution capabilities. Geophys. Res. Lett., 13: 697-700.

Marsh, J.G. and Martin, T.V., 1982. The Seasat altimeter mean sea surface model, J. Geophys. Res., 87: 3269-3280.

Mayes, C.L., 1988. Tectonic history and new isochron chart of the South Pacific. Master's Thesis, The University of Texas at Austin.

McAdoo, D.C., 1981. Geoid anomalies in the vicinity of subduction zones. J. Geophys. Res., 86: 6073-6090.

McConathy, D.R. and Kilgus, C.C., 1987. The Navy Geosat mission: an overview. John Hopkins APL Technical Digest, 8: 170-175.

Royer, J.Y. and Sandwell, D.T., in prep. Evolution of the Eastern Indian Ocean Since the Late Cretaceous: Constraints from Geosat altimetry.

Sailor, R.V. and LeSchack, A.R., 1987. Preliminary Determination of the Geosat radar altimeter noise spectrum. John Hopkins APL Technical Digest, 8: 182-183.

Sailor, R.V. and Okal, E.A., 1983. Applications of Seasat altimeter data in seismotectonic studies of the South-Central Pacific. J. Geophys. Res., 88: 1572-1580.

Sandwell, D.T., 1984a. A detailed view of the South Pacific geoid from satellite altimetry. J. Geophys. Res., 89: 1089-1104.

Sandwell, D.T., 1984b. Along-track deflection of the vertical from Seasat: GEBCO overlays. NOAA Technical Memorandum NOS NGS-40.

Sandwell, D.T. and McAdoo, D.C., in press. Marine gravity of the Southern Ocean and Antarctic margin from Geosat. J. Geophys. Res.

Sandwell, D. and Schubert, G., 1982a. Lithospheric flexure at fracture zones, J. Geophys. Res., 87: 4657-4667.

Sandwell, D.T. and Schubert, G., 1982b. Geoid height-age relation from Seasat altimeter profiles across the Mendocino Fracture Zone, J. Geophys. Res., 87: 3949-3958.

Scotese, C.R., Gahagan, L.M., and Larson, R.L., in press. Plate tectonic reconstructions of the Cretaceous and Cenozoic Ocean Basins, Tectonophysics.

Tapley, B.D., Born, G.H. and Parke, M.E., 1982. The Seasat altimeter data and its accuracy assessment. J. Geophys. Res., 87: 3179-3188.

60°N

30°N

0°

30°S

60°S

180°W

0°

180°E

Plate 1

(see page 40 for explanation)

Graduate Thesis

The vita has been removed from the digitized version of this document.